THE DEPOSITIONAL TIMING OF LOBATE LANDFORMS IN THE PARK AND LEON CREEK DRAINAGES WITH COMPARISONS TO WEST SALT CREEK LANDSLIDE, GRAND MESA AREA, MESA COUNTY, COLORADO

by

Omid Arabnia

A thesis submitted to the Faculty and the Board of Trustees of the Colorado School of Mines in partial fulfillment of the requirements for the degree of Master of Science (Geological Engineering).

Golden, Colorado

Date _____

Signed: _____

Omid Arabnia

Signed: _____

Dr. Paul M. Santi
Thesis Advisor

Signed: _____

Dr. Wendy Bohrson
Professor and Head
Department of Geology and Geological Engineering

ABSTRACT

The purpose of this research is to characterize two lobate deposits in the valleys adjacent to the West Salt Creek Landslide (WSCL) to assess whether these deposits can be used in magnitude/frequency hazard assessments of WSCL type failures. Present-day hazards cannot be assessed by looking at the deposits of the region without understand the process and timing that led to their deposition due to the many agents that shaped the Grand Mesa. The origin of the two lobate deposits is in question, as various authors have mapped them as debris flow, glacial, or bedrock deposits.

The two lobate deposits were dated and mapped using a variety of absolute and relative dating techniques, including radiocarbon and ^{3}He cosmogenic nuclide dating, Schmidt Hammer, pit-depths, lichenometry, and rind-thicknesses. Dating and mapping the lobes in each deposit allows for an understanding of the magnitude, frequency, and origin of each deposit. The combination of absolute dating methods shows that there is a lag time between deposition and accumulation of datable organic matter, suggestive of a glacial origin. The Park and Leon Deposits are found to be of Pinedale age, with the Park Deposit likely covering its entire valley in one event, and the Leon Deposit covering its valley in two events. The deposits are thought to be moraines, and therefore, should not be used in assessing WSCL type hazards. The Schmidt Hammer is found to be a low cost and reliable method to estimate relative ages of the glacial deposits in this region, whereas the other relative dating methods did not reflect the same conclusions reached by absolute dating. Pit-depths did not reflect deposit age due to the vesicularity of the basalts creating different starting points for pit-development depending on the original vesicle sizes. Rind-thicknesses have not appreciably developed because not enough time has elapsed since deposition. Lastly, lichen species present at the elevations investigated were not ideal for the age of the deposits.

TABLE OF CONTENTS

LIST OF FIGURES

LIST OF TABLES

CHAPTER 1

INTRODUCTION

The top of Grand Mesa, in western Colorado, is approximately 5000 ft (1524 m) above the major regional rivers (Yeend, 1969). The mesa cap is composed of many layers of basalt flows with a variety of ages, thicknesses, and erosive behavior. The basalt overlies a package of Cretaceous and Tertiary sedimentary rocks that has undermined the basalt as the relative height of the mesa surface and the surrounding rivers increased over time due to uplift of the Colorado Plateau and subsequent erosion (Cole and Sexton, 1981). Only a small portion of the basalt remains intact today, as most has failed and formed what is referred to as the landslide bench, whose edge lies at approximately ~9000 ft (2743 m) asl (Figure 1.1). In May 2014, the West Salt Creek Landslide (WSCL) occurred off the edge of the landslide bench, killing 3 people and depositing material over a square mile (2.6 km^2) (Figure 1.1). While landslides and debris flows are common in the area and cover as much as 39% of the surrounding region (Figure 1.2) (Soule, 1988), the scale and mobility of the WSCL was unprecedented in modern times for this region. In the valleys adjacent to WSCL, and at the same elevation, there are two deposits that are much larger than WSCL (Soule, 1988) (Figure 1.1 and 1.2). The two deposits, which will be referred to as the Park and Leon Deposits herein, are investigated in this study to judge their usefulness in predicting WSCL-type failures, as well the modern vulnerability of this region to Park/Leon type deposits. If these deposits were similar to WSCL in their mechanics, then they can be used in hazards assessments of WSCL type failures, such as for the East Salt Creek Drainage between the WSCL and the Leon Deposit (Figure 1.1 and 1.2). If the Park and Leon Deposits were similar to WSCL in their failure mechanism, it is likely that drainages like East Salt Creek, which is geomorphically and geologically similar to the West Salt Creek Drainage, are susceptible to this type of failure as well. However, if the Park and Leon Deposits are not mass failure deposits like the WSCL, then they are likely not useful for modern hazard assessments of drainages in this region.

Due to the many agents that have shaped the Grand Mesa since the deposition of the basalt around 9.45-10.99 Ma (Marvin et al., 1966; Cole et al., 2011), including volcanic, tectonic, colluvial, fluvial, glacial, glaciofluvial, lacustrine, and anthropogenic processes, it is difficult to assess present-day hazards by looking at the deposits of the region without understand the process and timing that led to their deposition. It is not clear whether the deposits Soule (1988) mapped as old debris flows, such as the Park and Leon deposits, are possible in today's climate and whether they should be incorporated in hazard assessments of WSCL-type failures. This is because it is not clear whether these deposits are gravitational mass failures, or of different origin such as glacial. Soule (1988) describes these deposits as originating from the top of the Grand Mesa from sediment packages left by the melting ice. Other authors suggest the deposits are till or bedrock (Yeend, 1969; Cole and Sexton, 1981).

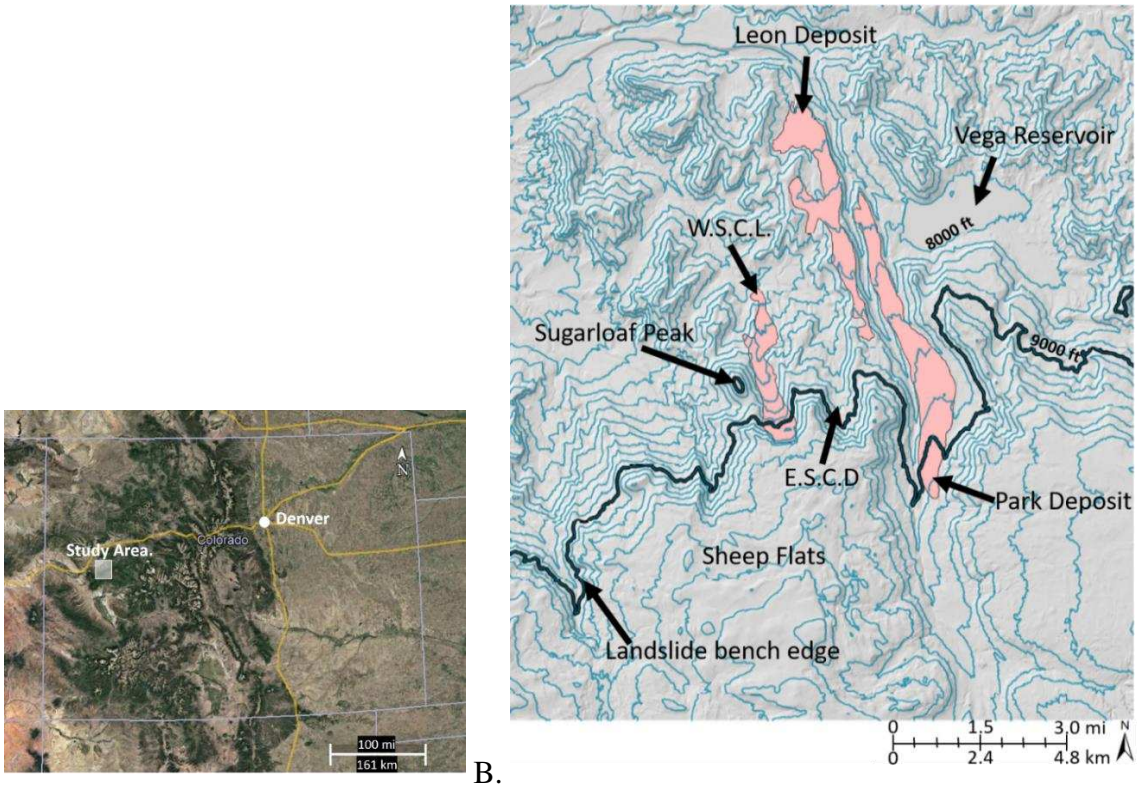

Figure 1.1 A) The location of the study area with respect to the state of Colorado. B) A topographic map with contour interval of 200 ft (61 m) shows the locations of the Leon, Park, West Salt Creek Landslide (W.S.C.L.) deposits and the East Salt Creek Drainage (E.S.C.D). Movement (downhill) direction is to the north. The boundaries of the Park and Leon Deposit are the same boundaries Soule (1988) used for debris flow deposits. The edge of the landslide bench is drawn at 9000 ft (2743 m) asl, which approximately corresponds to the boundary between the Wasatch Formation and the Green River Formation.

In addition to the process of deposition, the magnitudes of the deposits are unknown. Lobate features can be seen on both the Park and Leon deposits, which can be interpreted as either a single depositional event that covered the entire valley, like WSCL, or as an accumulation of episodic depositional events, where each episode deposits a lobe. To understand the depositing agent, depositional sequence, and magnitude of the Park and Leon deposits, a set of lobes from both were chosen for an absolute and relative dating study. This will aid in the understanding of whether WSCL was a unique mass failure event in its areal extent and runout, or whether failures of this magnitude were common for this region (Figures 1.1 and 1.2). Additionally, a set of relative dating techniques were implemented to judge which method allowed for the same conclusions to be reached as a valid absolute dating technique, which would offer a time- and cost-effective method for other researchers studying relative ages of deposits in this region.

A literature search, in conjunction with motivations to understand the mass failure deposits in this region, has led to the following questions and hypothesis for this research:

Questions:

1) Should the "odf" deposits mapped by Soule (1988) be used when assessing WSCL-type hazards (highly mobile, valley covering, long runout mass failures) for this region, such as magnitude/frequency relationships?
2) Is this region prone to Park- and Leon-type deposits in today's climate?
3) Did the Park and Leon Deposits cover their entire valley in one depositional event?
4) Are mass failures as prominent in the region as Soule's (1988) map suggests?

Hypotheses:

1) Geomorphic characteristics will show that the Soule (1988) odf deposits, such as the Park and Leon Deposits, are not analogous to WSCL and should not be used in assessing the regions hazard to WSCL-type failures.
2) Dating of the Park and Leon Deposits will show the region is not prone to similar deposits today because the region is no longer being actively glaciated.
3) The Park and Leon Deposits covered their entire valley in one depositional event.

4) Mass failures are not as prominent in the region as Soule's (1988) map suggests because the many deposits mapped as old debris flows are actually glacial deposits.

1.1 Geomorphology

The Grand Mesa region has been continuously shaped by volcanic, tectonic, colluvial, fluvial, glacial, glaciofluvial, lacustrine, and anthropogenic processes since the middle of the Miocene. Early research and mapping of the Grand Mesa focused on glacial deposits (Henderson, 1923; Nygren, 1935; Retzer, 1954; Yeend, 1969). Research then focused on surficial deposits, including landslides and debris flows (Soule, 1988), slump-block deposits (Baum and Odum, 1996), bedrock geology (Donnell et al., 1985; Hail 1972a, 1972b), and Quaternary deposits (Cole and Sexton, 1981). These maps generally show that since the deposition of the basalt, fluvial action and the Colorado Plateau uplift have inverted the topography, resulting in an elevated basalt platform flanked by landslides and pediment deposits. These pediments were deposited after about 3000 - 4000 ft (914 – 1219 m) of downcutting in the Pliocene (Yeend, 1969). The landslide bench formed after extensive slumping of the basalt cap due to undercutting of the weaker underlying sedimentary rock. The thickness of the basalt flows and the underlying gravel/claystone increases from 400 ft (122 m) thick in the west (where the cap is intact today) to 1600 ft (488 m) thick at Crags Crest to the east (Baum and Odum, 1996). This increase in thickness may have led to the increase of erosion from west to east on the landslide bench because the claystone is uncemented or weakly cemented and behaves plastically when remolded (Baum and Odum, 1996). Today, the landslide bench has many lakes and manmade reservoirs in the ridge and valley topography created by the large slump blocks.

After the topographic inversion and the formation of the landslide bench, the Grand Mesa region was reshaped again by a glacial icecap that was hundreds of feet (100+ meters) thick in areas (Yeend, 1969). Most of the surface glacial sediment covering the region is of Pinedale age (Yeend, 1969). The Pinedale initial advance is thought to have initiated in the Rocky Mountains around 30.2 +/- 1.2 kyr BP, reached its maximum extent around 22.4 +/- 1.1 kyr BP, and disappeared from the Front Range sometime before 11.8 kyr BP (Nelson et al., 1979; Legg and Baker, 1980; Madole, 1986; Benson, 2004). The deposits left by the ice are typically 0 – 10 ft (0-3 m) thick in much of the highland areas, and 10 – 98 ft (3-30 m) thick in moraines deposited

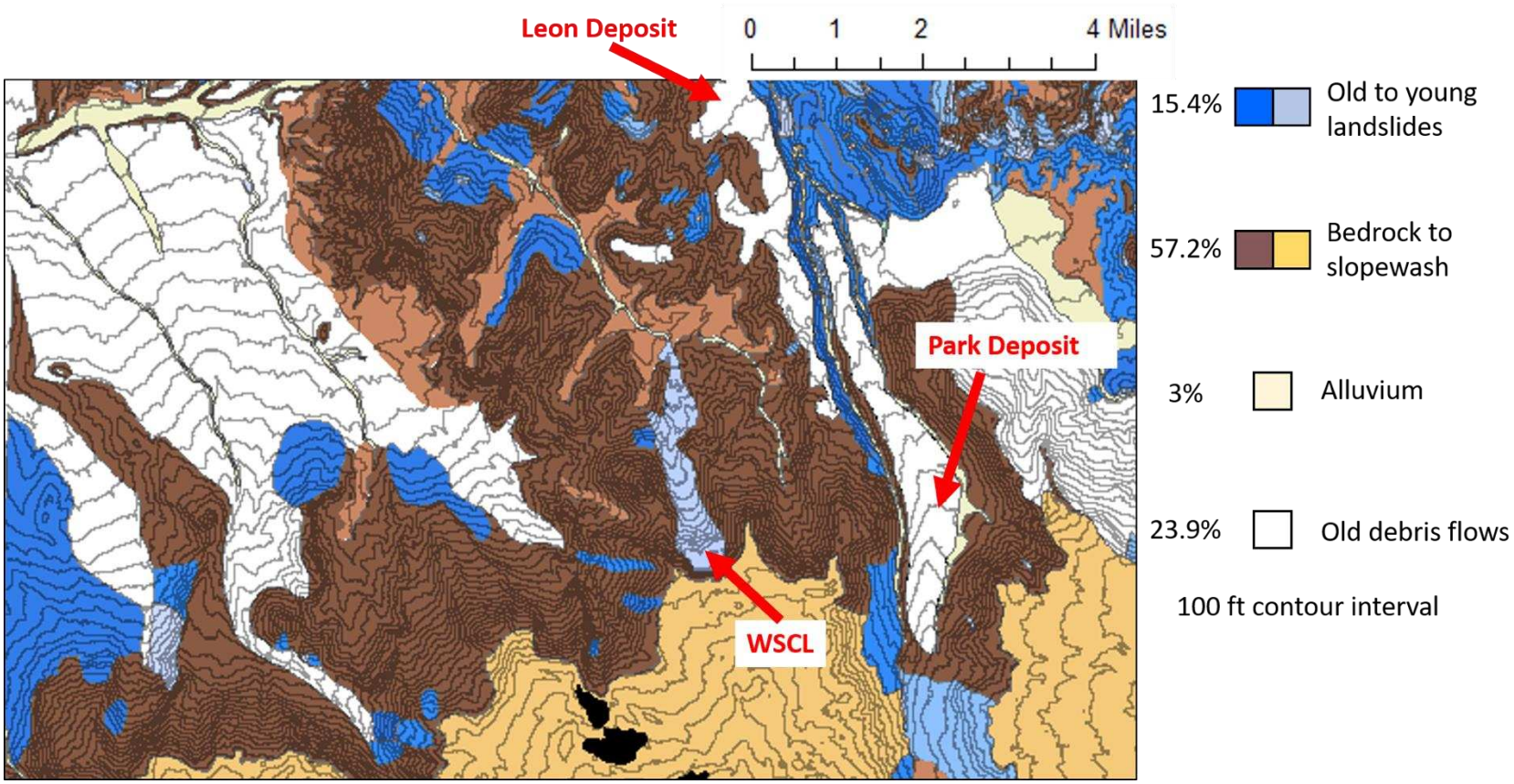

Figure 1.2 Deposit types in the region surrounding the WSCL, as mapped by Soule (1988) are color coded here. The percentages refer to the areal coverage of each deposit type.

between toreva blocks on Grand Mesa (Baum and Odum, 1996). The ice was most likely thicker on the north side of the Grand Mesa, where this study takes place, because of insolation.

The gradients off the mesa allowed the ice to form large ice tongues in the major valleys, especially the deep and narrow ones such as the Leon Creek drainage. Typically, these major valleys transition from till at high elevations to outwash at low elevations. Terminal moraines are rarely present (Yeend, 1969). Yeend (1969) gives an estimate of 5400 ft (1646 m) as the elevation for lowest extent of ice, where Cole and Sexton (1981) give a more conservative estimate of 6561 ft (2000 m) asl.

1.2 Geology

The alkali basalt flows that cap the Grand Mesa are part of stage 3 volcanism (11 – 9 Ma) associated with the uplift of the Colorado Plateau and Southern Rocky Mountains, as well as the genesis of the Rio Grande Rift (Cole et al., 2017). As many as 20 individual flows make up the 790 ft (240 m) of basalt (Cole and Sexton, 1981). Various layers of the basalt are thin and ravel to talus, while others are massive and form cliffs (Baum and Odum, 1996). The basalt could have covered as much as 500 mi^2 (1295 km^2), although only approximately 13% of the basalt from this stage of volcanism remains intact today (Cole et al., 2017). Interbedded with the Miocene basalt flows are intercalated tuff, baked soil horizons, and volcanic conglomerates (Marvin et al., 1966; Cole and Sexton, 1981). The only lithology present in the Park and Leon Deposits larger than gravel is basalt that originates from this basalt cap.

Beneath the basalt is a Paleocene through upper Eocene package of sedimentary rocks (Baum and Odum, 1996). These rocks dip gently to the northwest in the mapping area (Baum and Odum, 1996). The youngest rocks that make up this sedimentary package on the north side of the Grand Mesa are the Good Enough Formation, followed in increasing age by the Uinta Formation, Green River Formation, Wasatch Formation, Ohio Creek Formation, and the lastly the Mesaverde Formation (Table 1.1). These formations are mainly comprised of sandstones, siltstones, marlstones, shales, and conglomerates and make up the matrix of the Park and Leon Deposit

Table 1.1 Grand Mesa stratigraphy. Adapted from Yeend (1969).

System	Series	Formation	Member	Thickness in ft (m)	Rock Description
Tertiary	Pliocene	Intrusive and extrusive rocks		200-500 (61-152)	Basalt flows, dikes, and sills
	Pliocene (?)	Good Enough Formation		50-900 (15-274)	Gravel and variegated claystones
	Eocene	Uinta Formation		(?)	Fluvial beds of crossbedded sandstone
	Eocene	Green River Formation	Evacuation Creek	500 (152)	Light-brown and gray sandstone, gray marlstone, and siltstone
		Green River Formation	Parachute Creek	600 (183)	Black , brown, and gray oil shale that in places forms cliffs; contains minor amounts of gray siltstone and gray and brown fine to medium-grained sandstone
		Green River Formation	Lower	1,000 (305)	Fine to coarse-grained gray and brown sandstone, minor amounts of gray siltstone and marlstone, and few thin tan low-grade oilshale beds
		Wasatch Formation	Upper	400-1,600 (122-488)	Variegated shale and clay and some lenticular beds of sandstone, conglomerate, and limestone
		Wasatch Formation	Middle	0-400 (0-122)	Massive fine to coarse-grained gray and brown sandstone, in part conglomeratic; ledge former.
		Wasatch Formation	Lower	400-900 (122-274)	Variegated shale and clay and some lenticular beds of sandstone, conglomerate, and limestone.
		Unnamed Rocks		(?)	Brown and somber-colored shale with thin coal seams.
	Paleocene	Ohio Creek Formation		10-150 (3-46)	Massive fine to coarse-grained white to brown sandstone
	Upper Cretaceous	Mesaverde Formation		2,000-3,300 (610-1006)	Fine to medium grained ledge-forming brown sandstone interbedded with gray shale, carbonaceous shale, and thin coal beds.

1.3 West Salt Creek Landslide and the East Salt Creek Drainage

The WSCL was a rain-on-snow-induced event that initiated with its headscarp at the edge of the landslide bench (Figure 1.1). It traveled nearly 2.9 mi (4.7 km) with a mobility index (H/L ratio) of 0.14 (Coe et al., 2016). This is indicative of a highly mobile mass failure. In comparison, the Oso, Washington debris flow avalanche, that killed 43 people, had only a slightly longer mobility index of 0.105 (Iverson et al., 2015). The WSCL deposit covered a square mile (2.6 km^2) and mobilized 38 million yd^3 (29 million m^3) of sediment (White et al., 2015). It occurred in multiple surges as evidenced by seismic data (White et al., 2015; Coe et al., 2016), and without the assistance from the weight of the stratigraphically higher toreva blocks. However, an intact block of Green River Formation that was present at the top of the valley where the failure occurred has now back-rotated to form a depression that has since been filled to form a pond that later ruptured. A landslide was mapped by Soule (1988) at the headscarp prior to failure of WSCL in the Green River Formation (Coe et al., 2016) (Figure 1.3). Additionally, two more landslides were mapped along its flow path (Figure 1.3).

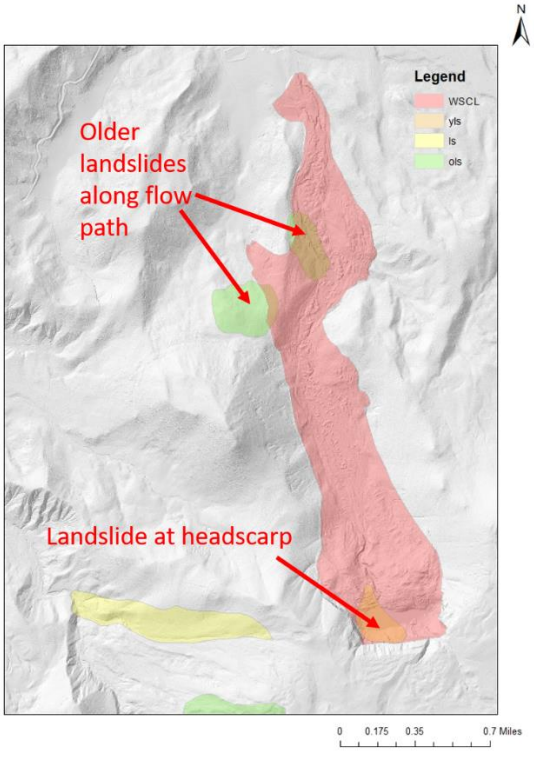

Figure 1.3 West Salt Creek Landslide is shown here, along with three landslides in its flow path and two in the immediate region. "ls", "yls", and "ols" are modern landslides, young landslides, and old landslides, respectively, as defined by Soule (1988).

The East Salt Creek Drainage (ESCD) and the drainage containing the WSCL are similar. Both have the same bedrock sequence, similar drainage areas, and similar gradients. However, the ESCD has no previous mapped failure or intact block of Green River Formation present. In addition, Yeend (1969) mapped extensive Pinedale Glaciation deposits in East Salt Creek, but not in West Salt Creek. It is important to understand if the Park Deposit, Leon Deposits, and WSCL, which surround the East Salt Creek Drainage are similar to one another in their depositing agent. If the deposits in the adjacent drainages to East Salt Creek are all mass failure, long runout, and valley covering deposits, it is possible that East Salt Creek may be susceptible to the same type of deposit. This is especially true since East Salt Creek and West Salt Creek drainages are similar geologically and geometrically. If the Park and Leon deposits are not modern mass failures like WSCL, and are glacial or glaciofluvial, then they are likely not useful for predictions of modern hazards such as in East Salt Creek.

1.4 Previous Researchers Descriptions of the Leon and Park Deposits

The Leon deposit was mapped by Soule (1988) as a debris flow that covers 1.6 mi^2 (4.1 km^2) and has a length of 4.1 mi (6.6 km). It has a relief of 1200 ft (366 m) and a H/L ratio of 0.055. In contrast to Soule's (1988) interpretation, Yeend (1969) and Cole and Sexton (1981) mapped the Leon deposit as Green River Formation. The Leon Deposit has been used for agriculture, thus many of the boulders that once scattered the deposit had been moved to strategic locations to allow easier access for farming equipment. Irrigation canals had been built across the deposit. All the Leon lobes are covered in grasses and shrubs.

The Park deposit was mapped by Soule (1988) as a debris flow that covers 2.1 mi^2 (5.4 km^2) of area, has a length of 5.2 mi (8.4 km), a relief of 1500 ft (457 m), and a H/L ratio of 0.055. In contrast, Cole and Sexton (1981) interpreted the Park deposit as glacial near the "head" and outwash at the "toe". Yeend (1969) maps the Park Deposit as Pinedale Glaciation age lower member till, although he acknowledges that the boundary between till and outwash is difficult to assess for this region. Yeend (1969) describes the valley containing the Park Deposit as the location of the longest glacial lobe in the area. The Park Deposit is continuous to the top of the Mesa where it is likely composed of deposits of glacial sediment. According to Yeend (1969), the glacial lobe likely dammed Plateau and Buzzard Creeks and produced a lake at the site of the modern Vega Reservoir. From here, the glacial lobe was predicted to have joined the thin ice

sheet originating from the Big Creek Drainage. After continuing down to Plateau Creek, it joined a glacial lobe originating in Cottonwood Creek, and stopped short of the Mesa Creek Drainage (Yeend 1969).

CHAPTER 2

METHODS

In order to understand the driving force and depositional timing of the Park and Leon deposits, the lobes were first mapped using desktop and field mapping techniques. After all possible lobes were identified and the boundaries outlined, a series of absolute and relative dating techniques was used on a set of the lobes. The lobes used in dating are chosen by taking into consideration the details of the dating techniques. For example, due to the necessity of in-situ boulders for ^{3}He cosmogenic dating, lobes on Leon where these boulders were moved cannot be dated using this technique. These types of considerations limited the possible choices for lobes for age dating. This was more applicable to Leon than Park because of the anthropogenic activity on the Leon Deposit. It was suspected that the combination of dating techniques provides a much better prediction than any technique alone. Each technique has its own uncertainties, assumptions, and sources of error that needed to be considered when evaluating the results and will be discussed further.

2.1 Field and Desktop Mapping

An iterative approach was implemented in the mapping of the individual lobes. A desktop map was first made using 2014 LiDAR data provided by the Colorado Geological Survey. The outer boundaries of Park and Leon Deposits were first assumed to match those mapped by Soule (1988). Lobes were outlined with their boundaries at concave regions that are topographically low points containing a convex surface and topographic low point. If a lobe could be identified using this criterion, even if it was not a prominent lobe, it was drawn as its own separate lobe. Therefore, gully formation post deposition could cause a deposit that was a single lobe upon deposition to be mapped as more than one lobe. The toe of each lobe was taken as a location with a slope break. Vegetative differences were not used in mapping because they were found to be unreliable in distinguishing lobes. For example, on the Park Deposit, the edge of the Aspen forest was at the crest of one of the lobes resulting in two vegetation types on one lobe.

After the completion of a preliminary desktop map, a field check of the map was undertaken. This consisted of walking the boundaries of lobes that do not have well defined low points on a topographic map in order to corroborate the desktop mapping. Lobes that were difficult to identify on the 10 ft (3 m), 20 ft. (6 m), or 40 ft (12 m) topographic maps were located in the field and incorporated into the map. Among the delineated lobes, 4 to 5 were chosen for further absolute and relative dating studies for each the Park and the Leon Deposits.

2.2 Absolute Dating

2.2.1 Radiocarbon Dating

Radiocarbon dating of bulk sediment was used to interpret the age of the deposits. Radiocarbon dating is an objective method for dating organic matter that can date deposits between 100 and 60,000 years old. This dating method takes advantage of the three naturally occurring isotopes of carbon, ^{12}C, ^{13}C, and ^{14}C. ^{12}C is the most common and stable of the isotopes. ^{13}C is also stable, but less common. ^{14}C makes up a very small percentage of the carbon in the atmosphere and is not stable, with a half-life of 5730 years. While an organism is living, the $^{14}C/^{12}C$ ratio is at equilibrium with the atmosphere. Following death, the unstable ^{14}C will begin to decay and the $^{14}C/^{12}C$ ratio of the dead organism will begin to deviate from the atmospheric $^{14}C/^{12}C$ ratio. By measuring this deviation, a radiocarbon date can be given to a sample. This can be done on a macro-particle or on bulk sediment. This study relies on radiocarbon dating of bulk organic matter in soil because no macro-particles, such as charcoal, were found.

Since bulk organic matter in soil was used in this study, and not individual macro-particles, it was important to understand if the organic matter tested has a wide range of ages present. Even within the same valley, there can be widely different aged organic molecules present in the soil that do not reflect the age of deposition (Ferguson, 1971). Some of the problematic carbon will make the depositional age appear younger than the actual age, such as those sourced from modern roots, organics in dissolved water, microorganisms, and soil fauna (Nowaczyk and Pazdur, 1990; Pessenda et al., 2001). Other sources of carbon can make the age of the deposit appear older than the actual age, such as dead trees in the path of the original flow that were entrained. Therefore, the uncertainty in the radiocarbon dates will be larger than if a macroparticle, such as charcoal, was dated. Quantifying this uncertainty is difficult. The most

stable and theoretically oldest organic fraction is the humin fraction (Wang et al., 2014; Pessenda et al., 2001; Balesdent, 1987; Becker-Heidmann et al. 1988). If the humin content has a much older age than the bulk organic matter, then contamination from modern day carbon or the entrainment of older carbon will be suspected. Therefore, the bulk organic matter and the humin content were both dated in two samples to test for the range of ages present in the organic matter dated. The two samples were chosen within the same valley, one in a grassy area and one in a forested area, to also understand how contamination differs as a function of vegetation.

The laboratory results were entered into the software Oxcal, which is a radiocarbon calibration program originally developed for paleoearthquake chronologies. This tool uses Bayesian statistics to incorporate all available chronological constraints (Lienkaemper and Ramsey, 2009). The results for radiocarbon ages are presented as probability distributions. A range of possible ranges exists for each radiocarbon measurement due to a couple different factors. The measurements of radiocarbon in tree rings, which is used to estimate ages of radiocarbon samples, have limited precision. Additionally, since atmospheric radiocarbon concentrations have varied overtime, it is possible to have several possible age ranges for each radiocarbon sample. Laboratory results are commonly reported as "BP" (before present, with present being the year 1950). Laboratory results reported as "BP" are based on a half-life assumption of 5568 years for radiocarbon and a constant atmospheric radiocarbon concentration over the time period in question. Oxcal calibrates the radiocarbon results to report a possible range and confidence for the true year of deposition, taking into account variability in atmospheric concentrations and uncertainties in tree ring data. In Oxcal, each lobe was treated as a "Phase", which forces no chronological ordering. Additionally, the R_Date function was used, which calculated a radiocarbon age for each sample.

It is important to note that, while absolute ages of the lobes were helpful to know, of most concern was the relative ages of the lobes (Question 3 and Hypothesis 3). Therefore, if younger or older carbon was incorporated into the deposits at equal rates, then the relative ages of the deposits should not be affected. This was considered a reasonable assumption when comparing lobes only within one valley and at the same depth, but not necessarily when comparing the Park Deposit to the Leon Deposit.

Samples were collected from holes dug using hand shovels, from a depth of two feet (61 cm). This depth ensured that we were within the deposit and not in areas of soil accumulation since deposition, although we suspected this would be very minor if at all present. The depth was kept consistent between samples to lessen any complications that would occur due to contamination differences at varying depths. The surfaces of the present-day deposits did not appear significantly altered since deposition, and therefore two feet (61 cm) was decided to be sufficient in depth to extract samples. Samples were sent to BetaAnalytic and DirectAMS for the dating of the bulk organic matter. Two samples were tested for humin content at BetaAnalytic in order to understand the range of ages in the organic compounds that make up the bulk organic matter. Beta Analytic reports that all results are accredited to ISO/IEC 17025:2005 Testing Accreditation PJLA #59423. Additionally, results were rounded to the nearest 10 years on individual samples following set conventions from the 1977 International Radiocarbon Conference.

Care was taken to remove any modern roots in the samples by both the author and the laboratory. The standard pretreatment methods were used at both laboratories for all samples except for samples where the humin content was dated. The pretreatment for bulk sediment was limited to an acid-only protocol to eliminate carbonates from the matrix. The remaining material was an aggregate value of all present organic carbon. The sample was sieved prior to pretreatment and all rootlets removed. The samples dated for humin content were treated with alkali to extract humic acids. This alkali extraction removed any unbound carbon that was alkali-soluble. The source of this carbon could be from more recent humic and fulvic acids or from ancient labile carbon that was alkali-soluble (BetaAnalytic results).

2.2.2 Cosmogenic Nuclide Dating

Several isotopes were considered for cosmogenic nuclide dating in this study. The more common isotope used in dating, ^{10}Be, could not be used due to the lack of quartz phenocrysts. ^{36}Cl on whole rock samples was considered for use in absolute dating, but its utility was not established due to laboratory delays. Additionally, after discussions with numerous researchers, it was concluded that the precision of whole rock samples would not aid in the separation of deposits by age, unless a large number of samples was dated. ^{3}He has a relatively high production rate and readily traps itself in olivine crystals, making it suitable for Holocene

deposits that contain basalt, such as Grand Mesa. (Kurz, 1986b; Craig and Poreda, 1986; Cerling, 1990; Cerling and Craig, 1994). Recent studies have improved the production rate determination because of well-constrained calibration sites (Blard et. al, 2013; Goehring et. al., 2010).

^{3}He can accumulate in a mineral in several ways, including cosmogenic, magmatic, and radiogenic processes. Only the cosmogenic ^{3}He is indicative of the deposit age, and therefore, the other sources (magmatic and radiogenic) of ^{3}He needed to be measured and subtracted from the total ^{3}He measurement (Marrero et al., 2016). Radiogenic ^{4}He can contaminate in olivine crystals through implantation (Lal et. al, 1989; Cerling et al., 1999). This additional ^{4}He decreases the ^{3}He/^{4}He melt ratio used to calculate the cosmogenic component, resulting in a determination of age that is younger than the true age of the landform (Cerling et al., 1999). Certain laboratory results help indicate if radiogenic contamination should be expected. If ^{3}He/^{4}He was less than one, or if ^{3}He/^{4}He was less in the furnace than in the crushed sample, this indicated contamination of a highly radiogenic component (Cerling, 1999). If the matrix proved difficult to remove from the olivine phenocrysts, radiogenic contamination should be expected. An abrasion technique was implemented in this study on a sample in order to test if the age of the outer layer of the olivine was contaminated through implantation. To do this, one of the samples was split in half, with half of the grains going through the abrasion process and the other half not. Then, both sets of samples were dated separately. Using this technique, a single value was estimated for the effect of radiogenic ^{4}He contamination on calculated cosmogenic dates to be used on all cosmogenic samples.

Magmatic ^{3}He is trapped upon solidification of the olivine mineral and is measured upon crushing in the laboratory (Kurz, 1986a). The magmatic contribution to the ^{3}He abundances was estimated using the crush ^{3}He/^{4}He ratios. The value used depends on the lobe in question due to a wide range of the crush ^{3}He/^{4}He ratios, which indicated variability in magmatic contribution to the estimated ages. Therefore, the most common method of calculating one magmatic contribution value to be used on all samples was not a valid method for this set of samples. It was better to estimate the magmatic contribution on a lobe by lobe basis for this set of samples, since the range in ^{3}He/^{4}He was much less within each lobe. A “best determination” was made for the magmatic value to be used for each lobe as recommended by Woods Hole Oceanographic Institute, which is the laboratory that completed the ^{3}He dating for this study.

Several criteria were used in the selection of boulders for cosmogenic dating. First, the boulders should be large, for two primary reasons. A large size increased the probability that the boulder had not been covered by snow or sediment for much of its past. It also increased the probability that the boulder had not been rolled since its deposition. For this reason, all sampled boulders had a b-axis over two feet (61 cm) and a minimum height above the ground of one foot (30 cm). Next, the boulders had a relatively flat sampling surface, which prevents self-shielding. If the surface of the boulder was at a low angle, the angle was recorded. However, most of the samples were taken from boulders with no slope on the top surface. Mossy areas were avoided, as were regions with prominent cracks. Boulders with abundant vesicles were not sampled (Cerling, 1999). The vesicles indicate that the lava flow solidified near the surface, and would therefore possibly start accumulating a cosmogenic signature when the boulder was part of the basalt cap. A better sample would be from the interior of the flows.

At each ^{3}He sample, latitude, longitude, and elevation were recorded using a hand-held geographic positioning system, and these values were used to calibrate laboratory results. The location was double checked using a Gaia application on an iPhone and a topographic map. The horizon was mapped for topographic shielding calculation using a Brunton compass. The Cronus Topographic Shielding Calculator version 2.0 was used to calculate the topographic shielding factor. No correction was made for snow shielding or radiogenic contamination because it was unlikely to be an accurate correction with the data that was available. It is important to note that with the incorporation of snow shielding, the calculated cosmogenic ages would be older than without snow shielding. Benson et al. (2004) found that the incorporation of snow shielding in cosmogenic dating samples increased the age of the sample by 12% in Pinedale deposits.

The results were calculated using the De scaling network using the Cronus software. The uncertainties were calculated in the Cronus software, which include those inherited from the AMS analysis, chemical concentrations, field measurements, production rates, scaling, and laboratory processing. The analytical uncertainty was calculated by fully propagating uncertainties on all inputs (Table 3.5). In contrast, the total uncertainty combined the analytical uncertainty and production rate uncertainty.

There are many ways that the calculated age for one individual sample may not reflect the correct age of the deposit, such as inheritance from previous exposure histories or radiogenic contamination. Therefore, three samples were collected for each lobe that was to be dated using cosmogenic nuclides. This increased the possibility of dating a basalt that has the same exposure age as the deposit itself. These samples were extracted with the use of hammer, chisel, and a battery powered drill. Since the sample surfaces was usually flat, at times the drill was needed to create a surface appropriate for chiseling. Samples were collected as small chips.

Olivine phenocrysts were extracted in the laboratory using a handheld steel cylinder for the delicate crushing of small samples of basalt without the loss of material. A hammer was used to strike the top of a steel cylinder to induce it to slide inside a casing that holds the basalt sample and crushes it with each blow. Light blows were used in order to not damage the olivine grains. Grains were then picked from the crushed rock material using tweezers underneath a magnifying glass. Most of the olivine grains were between 0.02 and 0.03 inches in b-axis. Grains were picked until there was at least 0.5 grams of phenocrysts to then be sent for dating at Woods Hole Oceanographic Institute. Samples were sent in small sets in order to ensure the method was valid before committing a large amount of resources. The laboratory results were then entered in version 2.0 of the Chronus Calculator to calculate ages.

2.3 Relative Dating

2.3.1 Schmidt Hammer Rebound Values

The Schmidt Hammer is an inexpensive, portable, and durable instrument that can be used as a relative age indicator. They have traditionally been used to measure the hardness of concrete by measuring the percentage rebound (R-value) after a steel rod is struck against the surface of interest at a known angle and known force. They have also been used as a tool to indicate the degree of weathering a rock surface has undergone and hence, the rebound values are a proxy for exposure age. For a given lithology, the rougher and more weathered the surface, the older it is, and the smaller R-value will be returned by the Schmidt Hammer. This method is appropriate to estimate relative ages for early to late Holocene deposits (Shakesby et al., 2006; Winkler, 2005). A few centuries (300 years) is commonly stated as the minimum time resolution for relative-age dating using the Schmidt Hammer (Matthews and Shakesby, 1984; McCarroll, 1987), although ages as low as 100 years have been claimed (Evans et al., 1999). This method

has been used in many environments including glacial, ramparts, avalanche, alluvial fan, and archaeological sites (Shakesby et al., 2006), and it was expected to be viable for the types of materials at WSCL and the vicinity.

The Schmidt Hammer was used on 25 boulders per lobe. The criteria used in the selection of boulders included a b-axis larger than 16 inches in order to limit the study to large, stable boulders. Initially, two operators were used, and two measurements were taken by each operator per rock holding the Schmidt Hammer perpendicular to the flat rock surface. This tested for operator bias and captured any spatial dependence for rebound values on the boulder. After the initial trip, it was judged that no operator bias existed, and therefore, only one operator was used on subsequent trips, but still 2 measurements were undertaken per boulder location. The surfaces were large and stable (Shakesby et al., 2006), clean, far from the edge of the boulder (Day and Goudie, 1977), comparable in lithology, dry (Sumner and Nel, 2002), flat, and free of lichen/visual fissures/cracks (Williams and Robinson, 1983; Sumner and Nel, 2002). Preliminary findings showed that vesicularity was a significant variable in the R-value, therefore, only nonvesicular rocks were sampled. Only basalt boulders were selected so any differences in rebound value would not be due to differences in lithology. The operator began at the toe of each lobe and walked towards the head, taking measurements of any boulder that met several criteria along the operator's path. If the toe was inaccessible, the operators chose the starting location to be the furthermost down-valley location that was accessible. Coordinates of each boulder were not recorded for this portion of the study.

Since the object of this part of the study was to estimate the relative ages of the deposits, a t-test was conducted between Schmidt Hammer results from each lobe. This indicated whether two populations of Schmidt Hammer values were statistically different. A p-value of <0.0500 was chosen as the threshold value to distinguish relative ages of deposits. If the p-value was less than 0.0500, than the two populations of Schmidt Hammer readings were considered to come from different populations. Then, the median and average values of those populations were used to order the lobes by age.

2.3.2 Rind-thickness Development

Weathering rind thicknesses was investigated for the usefulness in relative age dating as this technique has been used by other investigators for this purpose (McSaveney, 1992; Laustela, 2003; Colman and Pierce, 1981)). Rind-thickness depends on factors such as climate (precipitation and temperature), parent material, vegetation, topography, and time (Jenny, 1941; Colman and Pierce, 1981). Yeend (1969) matched weathering rind-thicknesses in the area with glacial deposits: for Bull Lake deposits, rinds averaging 1.39 mm in thickness were reported, for Pinedale glaciation, rind-thicknesses had a mean of 0.95 mm, and for late Pinedale, rinds had a mean of 0.06 mm.

Since Yeend (1969) found rinds in nearby locations, the basaltic rocks in the study area were expected to develop visible and consistent rind-thicknesses. Rinds develop through time due to weathering of iron bearing minerals (Carroll, 1974), common in the local basalt, forming a crust parallel to the rock surface (Colman and Pierce, 1981). In a basaltic rock, the rind will be yellow to reddish (Colman and Pierce, 1981). The fine-grained nature of basalt and mafic inclusions make them good candidates for the use rinds as a relative age dating technique because fine grained rocks develop a clearer weathering front than coarse grained rocks (Colman and Pierce, 1981).

Using rind thickness as a relative age indicator assumes that the rinds were not present upon deposition. This is a reasonable assumption for a glacial or debris flow deposit. Additionally, there is an assumption that the boulders and cobbles all experienced the same climate. Since all the lobes of interest to this study were in close proximity, this assumption was reasonably met.

Rind-thicknesses of exposed and shallow buried rocks were expected to be the same, and the rind thicknesses were expected to decrease with burial depth beneath the shallow rocks (Colman and Pierce, 1981; Porter, 1975). For younger deposits, surface and shallow rinds may be preferable because a larger delay exists between deposition and rind initiation for deeper rocks (Colman and Pierce, 1981). However, rind-thicknesses on surface boulders were probably more variable due to lichens (Jackson and Keller, 1970), fire, rolling by animals, uneven wetting, and erosion of weathered material (Colman and Pierce, 1981). Therefore, only surface and

shallow rocks were examined for rind-thicknesses, and caution was taken to avoid variability that may exist due to the listed complications. For example, rinds beneath lichens were not measured. Additionally, surface boulders with a b-axis smaller than two feet (61cm) were not examined to increase the chance that the boulder had been stable since deposition.

We used a drill and water to clear a hole large enough to investigate rinds on the surface boulders. In the holes dug for radiocarbon samples, subsurface cobbles were split by hammer and chisel to search for rind development down to two feet (61 cm) depth. Where no uniform rinds were found in the rocks, it was assumed that not enough time had passed for the rinds to develop in a way that would be useful in distinguishing the ages of the lobes present.

2.3.3 Pit Depths

Pits were investigated to judge their usefulness as a relative age indicator, as they have been used as a relative age indicator in many studies (Burbank, 1989; Carroll, 1974; Hereford et al., 1998). Pits occur due to a combination of acidic rainfall and metabolic activity of endolithic cyanobacteria (Hereford et al., 1998). Pit depths were measured from the bottom of the pit to a reconstructed upper surface following Carroll (1974). This provided a minimum pit depth since probably erosion has occurred on the edge or crest of the pit (Carroll, 1974). The count of pitted versus nonpitted boulders, and the depths of the pits on pitted boulders, were analyzed to assess their usefulness in distinguishing lobes of differing age. A boulder is considered pitted if it has at least one depression appearing to have formed due to grain by grain disintegration (Carroll, 1974), and without the aid of a vesicle. To be useful as a relative age indicator, it was important to compare pits that initiated either from the same size vesicles or from no vesicle at all. Since prediction of the initial vesicle size was not straightforward, care was taken to only examine pits that are thought to have initiated without the aid of a vesicle. Therefore, only nonvesicular rocks were examined to quantify the pitted versus nonpitted ratios and the pit depths. The largest pit was recorded for each rock analyzed. On lobes where pits were examined, the first 25 nonvesicular boulders found were recorded to calculate pitted versus nonpitted ratios, and additional boulders were examined until 25 pitted boulders were found to measure pit depths.

2.3.4 Lichenometry

The lichen species in the area were investigated in order to see if they could be of use as an age indicator for the Park and Leon deposits. Ideal species are slow-growing crustose species growing on a hard rock surface such as rhizocarpon geographicum (Benedict, 1968; Carrara and Andrews, 1972). If located on a soft surface, there was risk of erosion. Flaky species were too vulnerable to damage to be of use for older deposits. At each location aspect, elevation, and the largest lichen diameter per boulder, and percent lichen cover should be recorded following previous investigators methods (Benedict, 1968; Mahaney, 1973; Carrara and Andrews, 1973; Carroll, 1974; McCarthy, 2001). Only circular or oval lichens were sought out. Diameter would be measured for the a- and b-axis of the lichen, to the nearest hundredth mm using a Mitutoyo CD-P6S digital caliper with measurement uncertainty of +/- 0.02 mm.

This method assumes that the surface was lichen free at the time of deposition. This assumption would be reasonable whether the deposit is debris flow or glacial in origin. Additionally, the lobes were all at similar elevations and in close proximity, so no variation in climate was expected. Species such as lecidea atrobrunea or rhizocarpon geographicum were sought out for this method.

2.4 Scope of Research

The research questions were addressed by focusing on three main canyons: West Salt Creek and the detailed studies following its movement in 2014, and the nearby parallel canyons containing Park and Leon Creeks above Vega Reservoir, which were mapped together as a long "odf" by Soule (1988). Since East Salt Creek is located between West Salt Creek and the Park/Leon canyon area, it is briefly discussed. The overall goal was to carefully characterize the Park/Leon Deposits to understand if they were similar to the West Salt Creek failure. If so, this information would be extended to assess the vulnerability of East Salt Creek to this type of failure, which was morphologically similar to West Salt Creek and was a candidate for the same type of failure. The research questions and hypotheses corresponded to three main tasks completed for the project.

Task 1: Detailed Mapping

The first task delineated the extent of the lobes that make up the Park and Leon deposits, which will be used in interpretation of the deposit origins and in evaluating question #3 and #4 and hypothesis #1, #3, and #4.

The project area was defined as an approximately 15 mi^2 (10.6 km^2) region bounded by West Salt Creek to the west and Park Creek Canyon to the east. Park Creek Canyon was accessible by public road. Leon and East Salt Creek Canyons were linked by BLM land, and all canyons were linked at higher elevation by National Forest land. Access to private land on the Leon Deposit was granted by from the Ute Water Conservancy District.

The individual lobes making up the Park and Leon Deposits were mapped at 1:24,000 scale. Mapping proceeded with iterative office (air photo and LiDAR) delineation and confirmatory field work. Stereo aerial photography and LiDAR for the area was available from CGS.

Task 2: Event Size and Timing

In order to evaluate whether the Park/Leon area was a single, large event, or several smaller events that moved at different times (question #3) a staged investigation was completed as follows:

Stage 1 - Detailed mapping of the area (task #1) identified whether there were multiple flow lobes at the surface, which possibly indicated that the deposit was developed by multiple events over time.

Stage 2 – With multiple lobes present on both the Leon and the Park Deposit, we collected three cosmogenic dating samples from exposed boulders on each of two Park Deposit Lobes, and three radiocarbon sample per lobe from hand dug holes on four Park Deposit Lobes and 4 Leon Deposit Lobes. In addition, a suite of relative dating techniques was attempted including Schmidt Hammer readings from boulders, lichen sizes, rind-thicknesses, and pit depths on exposed and buried boulders. These dating techniques help answer question #3, as well as test hypotheses #2, and #3.

Task 3: Glacial / Debris Flow Deposit Assessment

An assessment was made on whether the Leon and Park Deposits are glacial or debris flow deposits (question #1, #2, #4, and hypothesis #1, #2). This was done using previous maps for this region (Yeend, 1969; Cole and Sexton, 1981; Soule, 1988). In addition, the results from the different dating techniques were used to infer the depositional process by understanding the climatic conditions at the time of deposition. Features indicative of a glacial origin (striations, eskers, kettles, outwash, moraines, and drumlins) and debris flow deposition (levees, coarse snout, and fans) were sought out in the field. The mobility indices were compared to other mass gravitational failures. Additionally, absolute dating was used to investigate whether a lag time exists between deposition and carbon accumulation in the deposit.

Task 4: Prediction of Future Hazards

Using the information from Tasks 1-3, we assessed whether the "odf" deposits mapped by Soule (1988) should be used in predicting WSCL-type hazards, such as in East Salt Creek (question #1 and hypothesis #1). If Park/Leon Canyons behaved like West Salt Creek, then it is possible that East Salt Creek will behave similarly. If Park/Leon are different, then other geomorphic and topographic indicators are needed assess the future behavior at East Salt Creek.

CHAPTER 3

RESULTS

3.1 Field and Desktop Mapping

Using the criteria established in section 3.1, a lobe map was constructed for both the Park and the Leon Deposits (Figure 3.1 and Figure 3.2). A total of 15 lobes within the Leon Deposit, and a total of 9 lobes within the Park Deposit were identified (Figures 3.1 and 3.2). If the entire deposits were considered to be one event, the Leon and Park Deposits were much larger than WSCL in both their areal coverage and their runout length (Table 3.1). The relief of WSCL, in contrast, was 650 to 950 ft (198 to 290 m) greater than the Leon and Park Deposits, respectively (Table 3.1). With the much greater relief and shorter runout, WSCL had a mobility index (H/L) that was a factor of 2.5 times larger than the Leon and Park Deposits (Table 3.1).

Table 3.1 Leon, WSCL, and Park Deposit Properties.

	Leon Deposit	WSCL	Park Deposit
Areal Coverage	4.1 km^2 (1.6 mi^2)	2.6 km^2 (1 mi^2)	5.4 km^2 (2.1 mi^2)
Runout	6.6 km (4.1 mi)	4.7 km (2.9 mi)	8.4 km (5.2 mi)
Relief	366 m (1200 ft)	655 m (2150 ft)	457 m (1500 ft)
Mobility Index (H/L)	0.055	0.14	0.055
Mapped as…	Bedrock or debris flow	-	Debris flow or glacial

Much of the Park Deposit was forested by aspen (lobes P1 and P4 in Figure 3.2). Lobes P2 and P3 were not forested and were covered by grasses and shrubs (Figure 3.2). There were abundant boulders found on the surface of all Park Deposit lobes with b-axis larger than three feet (91 cm). These boulders were easy to spot on the grassy sections, and usually occured on the convex portion of the lobes. Cobbles and boulders were found in all the two feet (61 cm) deep holes dug for radiocarbon samples, suggesting the deeper deposit was made of the same

material as on the surface. Soil formation since deposition was very limited even in the forested areas.

The Leon Deposit was found to be much more anthropogenically disturbed than the Park Deposit. However, there were basalt boulders larger than three feet (91 cm) in diameter scattered in many undisturbed areas in a similar way as on the Park Deposit. These basalt boulders were miles from the Grand Mesa surface and at the same elevation as the transported material in the Park Deposit. Close field observation by the author concluded that the Leon Deposit was of transported material and not bedrock, because the surface sediment and bedrock were different lithologies. Many basalt boulders were present on the surface and buried on all the Leon Lobes examined, and the closest basalt bedrock was the Grand Mesa caprock. Lobe L3 had sections that had not been disturbed due to its very close proximity to steep valley edges which had prevented farming (Figure 3.1). Even in the farmed areas, boulders and cobbles were only inches beneath the present-day ground surface, suggesting that the modern anthropogenic activity had not disturbed the deposit more than inches below the surface.

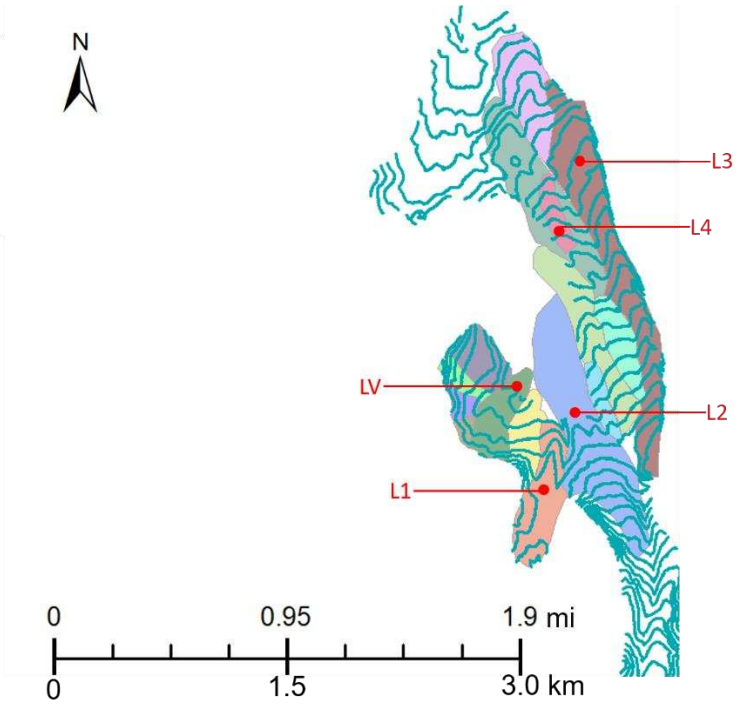

Figure 3.1 Lobes within the Leon Deposit are shown in different colors on a topographic map with 20 ft (6 m) contour interval. The lobes evaluated with absolute and relative dating techniques are labeled.

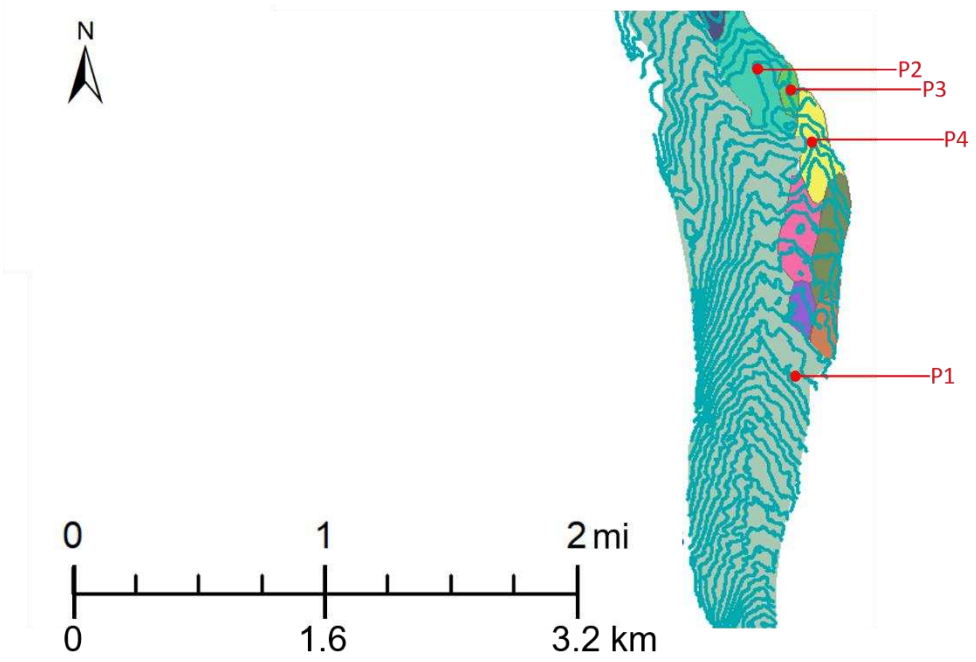

Figure 3.2 Lobes within the Park Deposit are shown in different colors on a topographic map with 20 ft (6 m) contour interval. The lobes evaluated with absolute and relative dating techniques are labeled.

The boulder deposition on lobe LV was unique when compared to lobes L1-L3. Most of lobe LV was cleared of surface boulders to prepare the land for agriculture. The boulders that were present on LV are located at the "toe", just as the elevation increases slightly on a hill-like feature. Sedimentary clasts were found in a hole dug on this hole. No sedimentary clasts were found on any other lobes on either the Park or Leon Deposits. It seemed that the hill decreased the energy of the material being transported enough to cause deposition. The boulders were more clearly imbricated than at other locations on the Leon Deposit (Figure 3.3).

The lobes mapped on both Leon and Park showed no braiding or sorting. The lobes were consistently linear in shape. Additionally, the elevations of the lobe crests were all at approximately the same elevation as the other lobes within each valley. Of all the lobes present on the Park and Leon Deposits, lobe P1was the largest by a significant margin. This lobe extended continuously in the up-valley direction to the top of the Mesa, which was the sediment source for these flows. In contrast, the Leon lobes do not have a single clear source area, and in fact, as each lobe was traversed in the up-valley direction, it appeared that there were two

possible source areas. Lobes L1 and LV appeared to have a different source area than lobes L2, L3, and L4.

Figure 3.3 Imbrication on lobe LV.

Several interesting features were found on these deposits that were suggestive of the driving force behind their deposition. P2 had two dry features and P1 has many swampy features that can be interpreted as kettles. Most of the features are on lobe P1 and tend to be circular in shape (Figure 3.4). This is suggestive that lobe P1, and possibly P2, had isolated, stagnant ice blocks that were then surrounding by outwash. Therefore, this region may be a transition zone between glacial and glaciofluvial deposits for lobe P1. However, evidence down-valley from

this area was not suggestive of a deposit that was dominated by the outwash that would be expected downstream of glaciers. Similar features were not found on the Leon Deposit. In addition, within lobe P4 there appeared to be a toe where there was a sharp slope break. Down-valley of this slope break there appeared to be another deposit that was buried by lobe P4. These two deposits were mapped as one lobe because there was no other distinguishing feature to suggest that the underlying lobe was a different flow, other than a slight increase in the frequency of large boulders on the underlying deposit, but not an increase in their size.

3.2 Absolute Dating

Radiocarbon dating and cosmogenic nuclide dating results are reported below.

3.2.1 Radiocarbon Dating

Radiocarbon sample locations are mapped in Figure 3.5 and 3.6 or the Leon and Park Deposits, respectively.

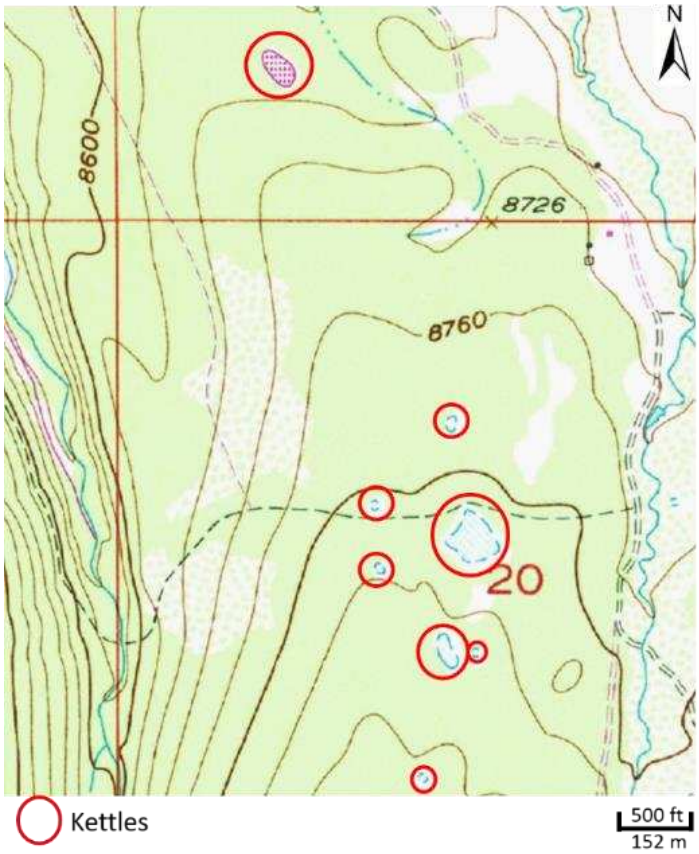

Figure 3.4 Locations of kettle-like features on the Park Deposit.

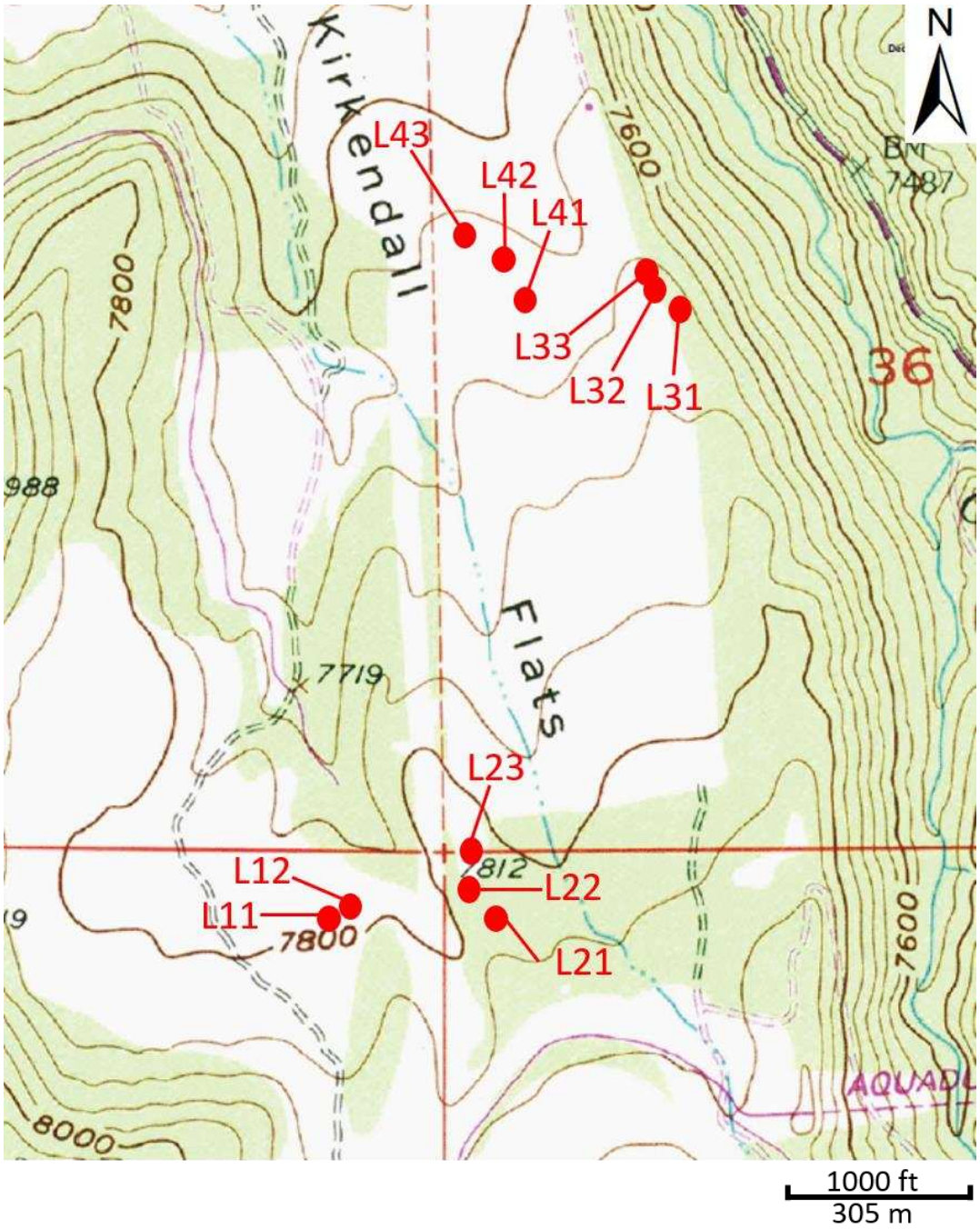

Figure 3.5 Radiocarbon sample locations for the Leon Deposit.

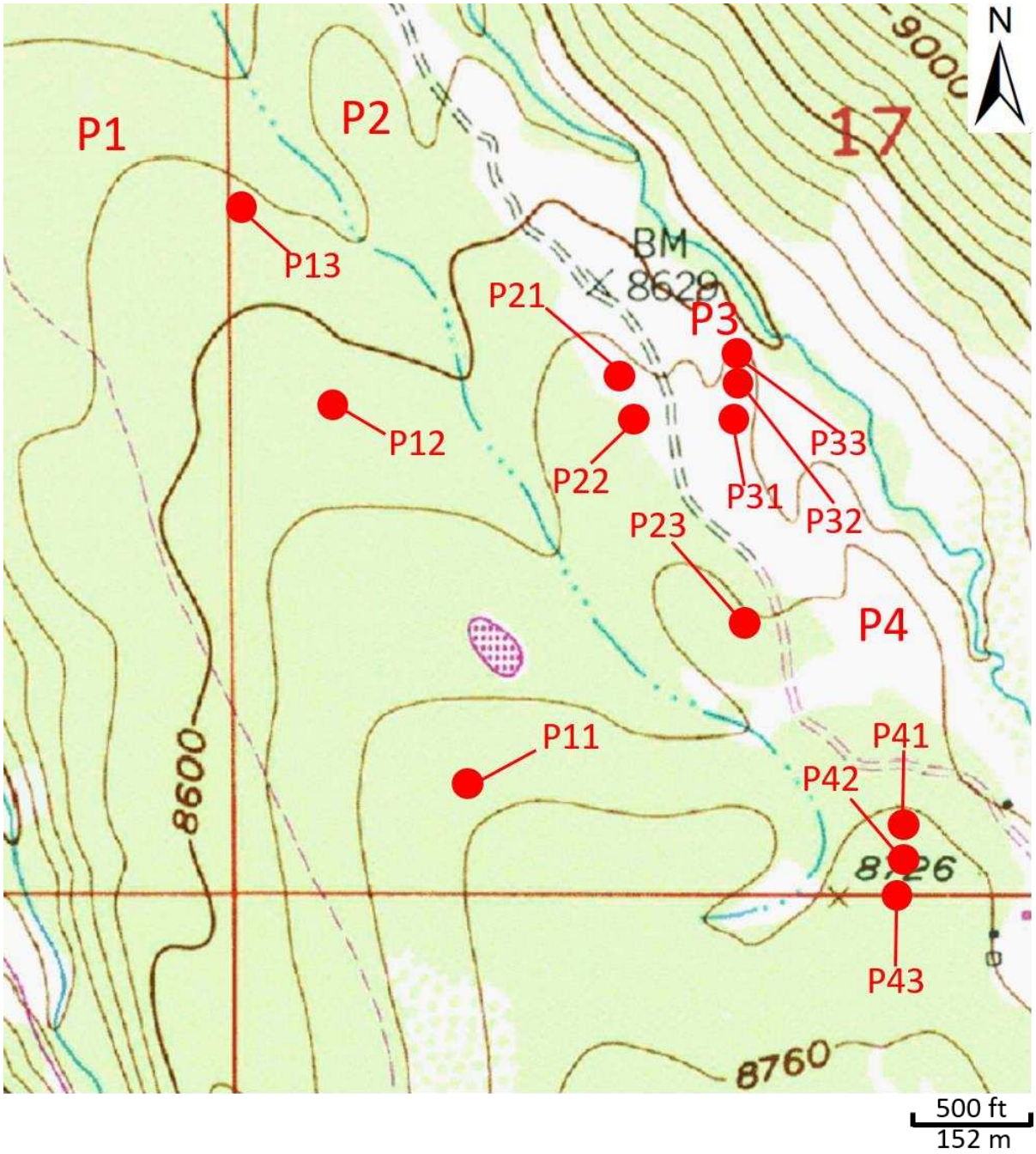

Figure 3.6 Radiocarbon sample locations for the Park Deposit.

All reported conventional radiocarbon ages have been corrected for total fractionation effects (Tables 3.2 and 3.3, Figures 3.7, 3.8, and 3.9). Uncertainties of +/- 30 years were reported for all ages by the laboratories. These will be discussed more in section 6.2.1.

Table 3.2 Conventional and calibrated radiocarbon age of all samples. The 95% confidence interval ages are calculated using the Oxcal software. Samples P22H and P23H are dated using humin content.

Lobe ID	Sample ID	Conventional Radiocarbon Age (BP)	95% confidence interval lower bound (BC/AD)	95% confidence interval upper bound (BC/AD)	Latitude (North)	Longitude (West)
L1	L11	3955	-2570	-2346	39.22507	107.84152
L1	L12	3381	-1746	-1616	39.22528	107.84111
L2	L21	2663	-895	-796	39.22519	107.83832
L2	L22	2168	-360	-115	39.22543	107.83879
L2	L23	2369	-539	-388	39.22588	107.83869
L3	L31	1707	252	400	39.23463	107.83498
L3	L32	2776	-1001	-842	39.23479	107.83533
L3	L33	2807	-1048	-859	39.23490	107.83538
L4	L41	4016	-2618	-2470	39.23529	107.83884
L4	L42	4394	-3096	-2916	39.23503	107.83796
L4	L43	4122	-2866	-2580	39.23452	107.83760
P1	P11	1930	4	131	39.18229	107.80218
P1	P12	1580	410	546	39.18649	107.80426
P1	P13	1060	897	1024	39.18878	107.80548
P2	P21	2097	-196	-46	39.18675	107.79982
P2	P22H	1750	222	385	39.18641	107.79967
P2	P22	1637	339	535	39.18641	107.79967
P2	P23H	520	1324	1443	39.18407	107.79822
P2	P23	666	1276	1392	39.18407	107.79822
P3	P31	1661	260	528	39.18635	107.79839
P3	P32	1702	252	405	39.18673	107.79826
P3	P33	2373	-702	-389	39.18713	107.79829
P4	P41	1676	258	424	39.18176	107.79585
P4	P42	2137	-352	-55	39.18127	107.79588
P4	P43	2139	-353	-56	39.18100	107.79603

The radiocarbon results are graphically represented with the average age for each deposit also plotted (Figure 3.7). These average ages are listed in Table 3.3. Oxcal results are plotted in Figure 3.8 (Park Deposit) and Figure 3.9 (Leon Deposit).

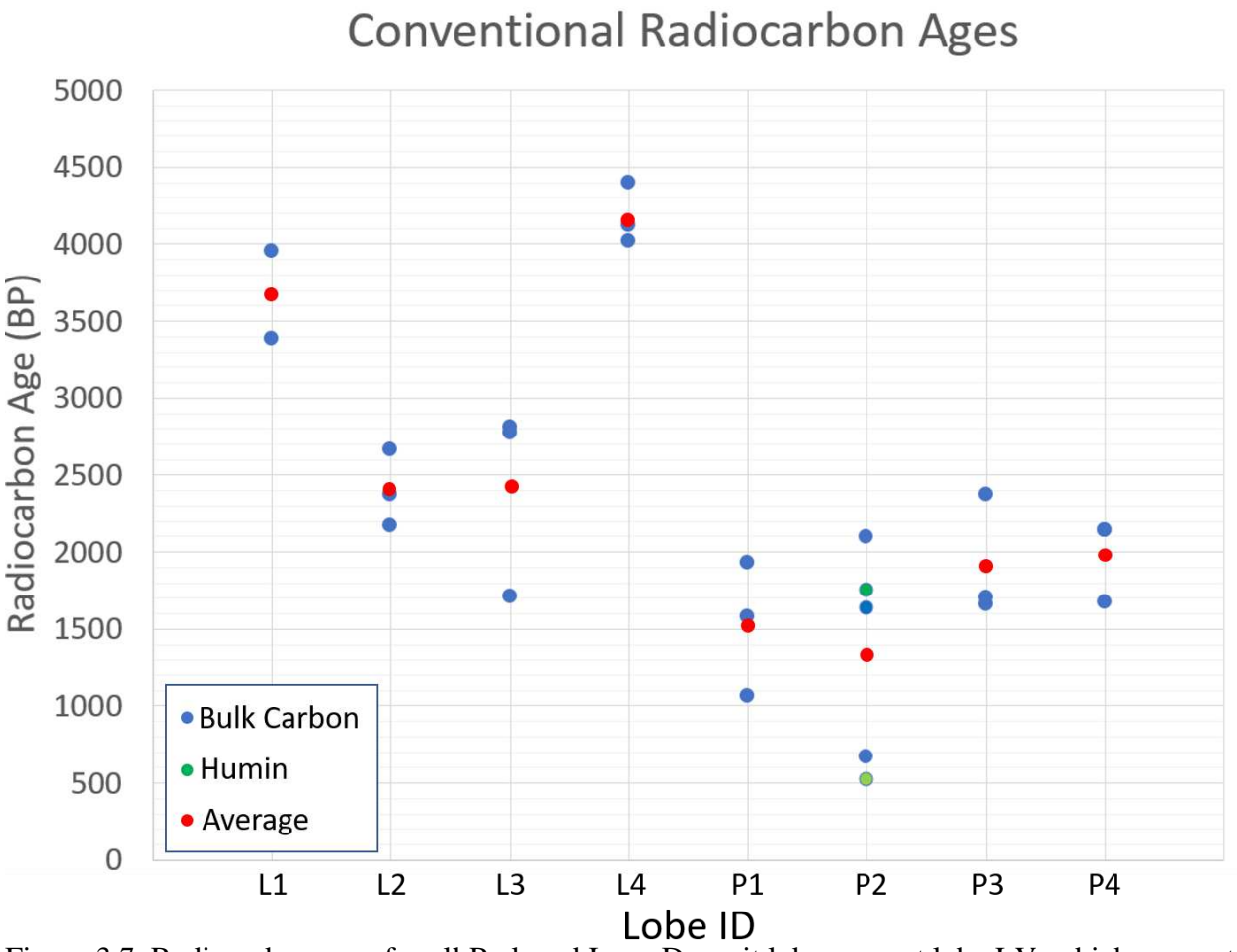

Figure 3.7 Radiocarbon ages for all Park and Leon Deposit lobes except lobe LV, which was not dated using radiocarbon. Bulk carbon, humin, and average dates are plotted for each lobe.

Table 3.3 Average radiocarbon ages.

Lobe ID	Average Age (BP)
L1	3668
L2	2400
L3	2430
L4	4177
P1	1523
P2	1334
P3	1912
P4	1984

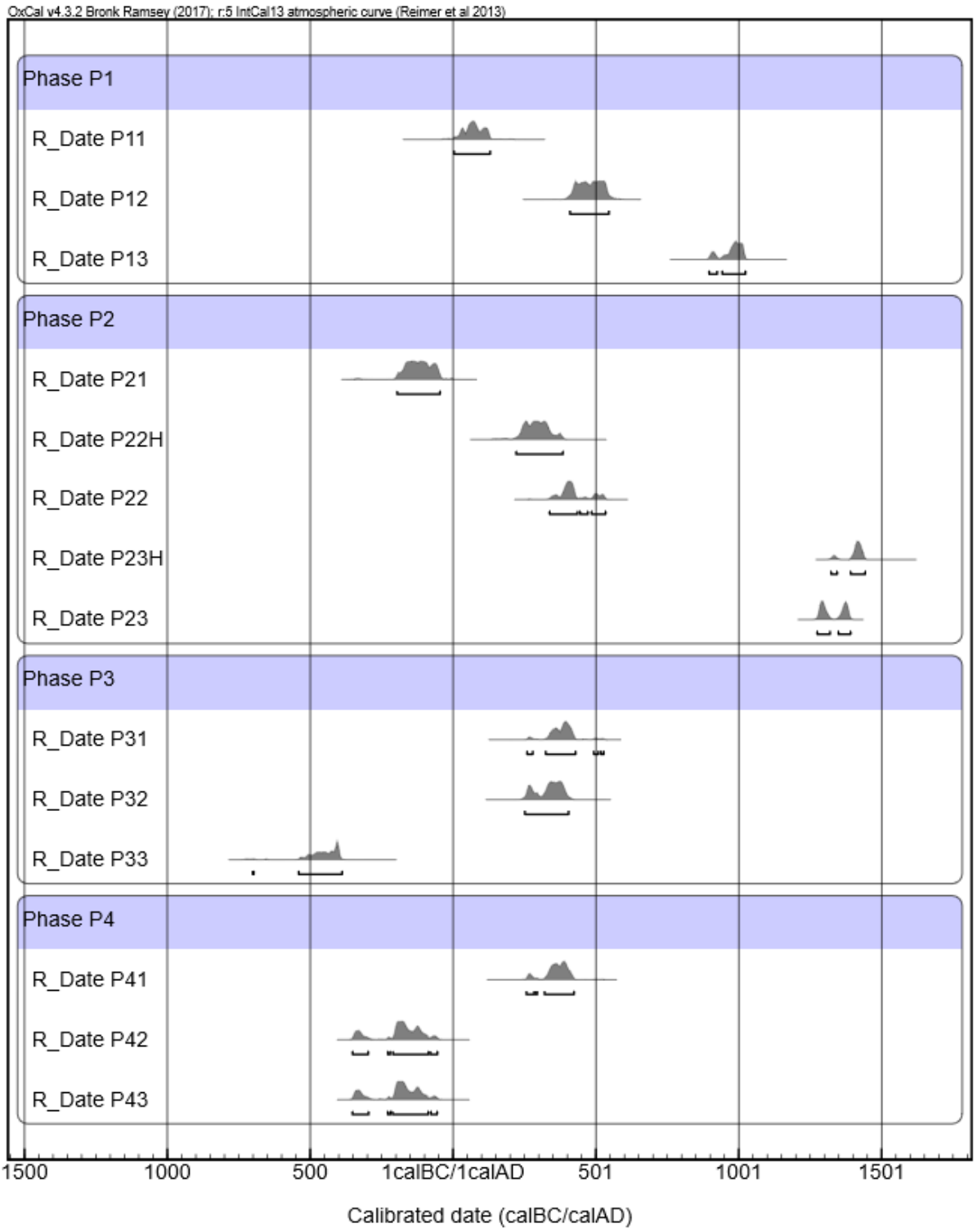

Figure 3.8 Summary output for the Park Deposit radiocarbon ages in Oxcal. The probability density functions for each date are shown. The bars below the probability density functions indicate the 68 and 95 percentile confidence ranges. The higher the histogram, the more likely that age is. Phases correspond to individual lobes, and R_Dates correspond to specific radiocarbon samples.

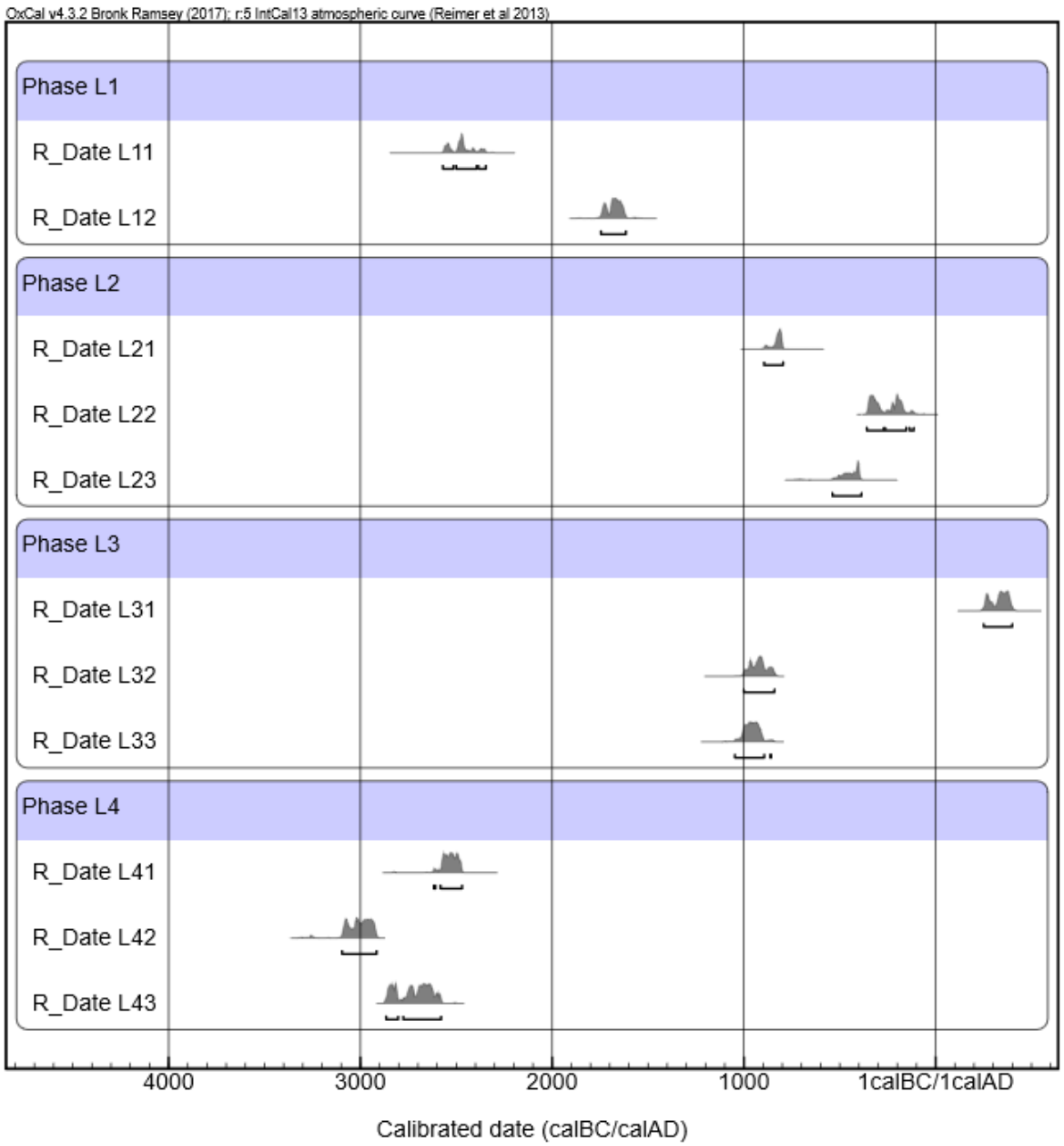

Figure 3.9 Summary output for the Leon Deposit radiocarbon ages in Oxcal. The probability density functions for each date are shown. The bars below the probability density functions indicate the 68 and 95 percentile confidence ranges. The higher the histogram, the more likely that age is. Phases correspond to individual lobes, and R_Date correspond to specific radiocarbon samples.

The Park Deposit lobes are estimated to have deposited at the same time using the age ranges and averages (Figure 3.7 and 3.8; Table 3.3). Adjacent lobes (P1/P2, P3/P4) had much closer radiocarbon ages than the nonadjacent lobes. Average ages for P1 and P2 were separated by 189 years, and average ages for P3 and P4 were separated by 72 years. In contrast, not all

Leon Deposit lobes appear to be the same age using the ages ranges and averages (Figure 3.7 and 3.9; Table 3.3). Lobes L1 and L4 appear to have distinctly different ages (older) than lobes L2 and L3. However, there are not enough tested samples to calculate a detailed statistical comparison. The magnitude of the range of ages seen on the Leon Deposit was nearly 4 times the range calculated for the Park Deposit. Therefore, it was estimated that the Leon Deposit consisted of two depositional events. Lobe LV was not dated using radiocarbon dating. This was because the boulders residing on the LV are transported sediment, however, the underlying sediment was suspected to be of bedrock origin because this was the only lobe in which clasts of sedimentary rocks were found on either the Park or the Leon Deposit

3.2.2 Cosmogenic Nuclide Dating

Examples of the sampled boulders for cosmogenic nuclide dating are shown in Figure 3.10. Dating of lobes P1, P2, and LV was attempted using the cosmogenic technique (Figure 3.11).

Figure 3.10 Examples of boulders sampled for cosmogenic nuclide dating.

A.

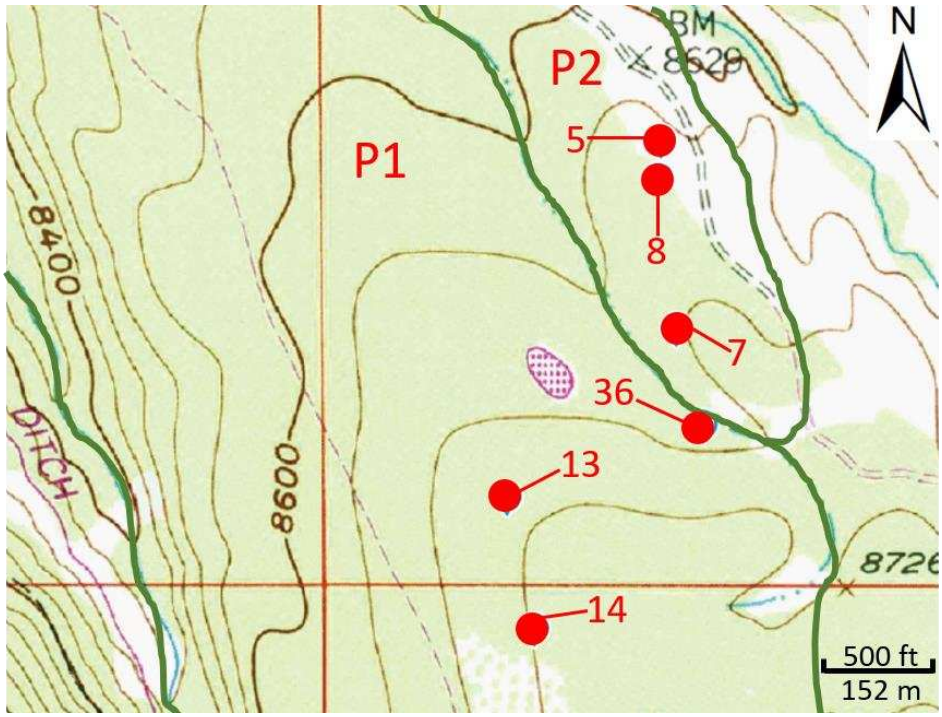

B.

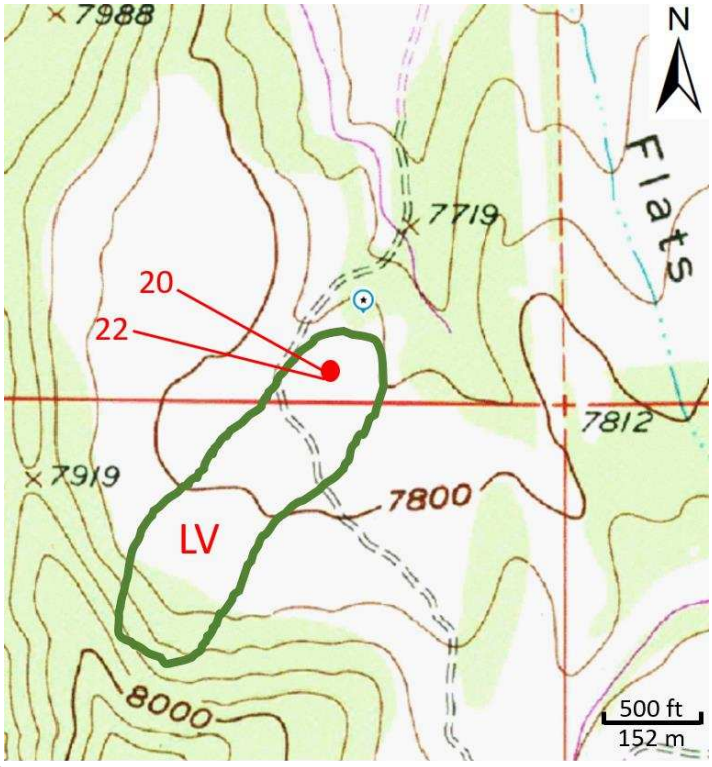

Figure 3.11 A) Park Deposit cosmogenic nuclide sample locations. B) Leon Deposit cosmogenic nuclide sample locations.

The raw ^{3}He cosmogenic nuclide dating results from Woods Hole Oceanographic Institute are reported below (Table 3.4). The sample "13 clean" refers to the sample which was abraded in order to remove the outermost layer of the olivine grains to test for radiogenic contamination on the mineral surface.

Table 3.4 Raw laboratory cosmogenic nuclide results.

Sample Name	Weight (g)	$^{3}He/^{4}He$ (R/Ra)*	Sigma (R/Ra)*	^{4}He in MS (cc STP)	4He (cc STP/g)	Fraction Crush
5 crush	0.25471	3.55	0.48	5.75E-11	2.26E-10	
5 furnace	0.24486	12.71	0.29	6.88E-09	2.81E-08	0.0080
7 crush	0.19726	3.05	0.89	1.36E-10	6.90E-10	
7 furnace	0.18554	8.41	0.13	1.02E-08	5.48E-08	0.0124
8 crush	0.19189	4.19	0.48	4.81E-11	2.50E-10	
8 furnace	0.18061	16.04	0.36	1.02E-08	5.65E-08	0.0044
13 clean crush	0.17465	4.39	0.97	1.32E-10	7.56E-10	
13 clean furnace	0.15924	37.66	0.72	1.41E-09	8.88E-09	0.0785
13 crush	0.24757	4.53	0.57	2.55E-10	1.03E-09	
13 furnace	0.23326	20.62	0.31	3.94E-09	1.69E-08	0.0576
14 crush	0.24151	6.13	0.18	1.17E-09	4.85E-09	
14 furnace	0.22914	4.59	0.10	1.99E-08	8.68E-08	0.0529
20 crush	0.26625	2.23	0.89	2.52E-11	9.47E-11	
20 furnace	0.25279	4.38	0.10	3.49E-08	1.38E-07	0.0007
22 crush	0.27393	1.07	0.45	6.63E-11	2.42E-10	
22 furnace	0.25063	5.13	0.12	2.27E-08	9.07E-08	0.0027
36 crush	0.2371	3.62	0.34	6.86E-11	2.89E-10	
36 furnace	0.2258	11.73	0.27	5.52E-09	2.44E-08	0.0117

*Ra=1.384 x 10^{-6}

The inputs into Cronus are shown below (Table 3.5). The shielding factor refers to topographic shielding. No snow shielding was incorporated into these results because enough data does not exist to reliably estimate the snow depth over the period of time in question.

Table 3.5 Cronus inputs for ^{3}He cosmogenic nuclide samples.

Sample Name	Latitude (North)	Longitude (West)	Elevation (m)	Shielding Factor	Conc. ^{3}He (10^{7} at/g)	Conc. ^{3}He Sigma (10^{7} at/g)
5	39.18568	107.79916	2647	0.99476	1.010	0.0980
7	39.18697	107.79946	2645	0.99638	1.091	0.1830
8	39.18640	107.79920	2658	0.99638	2.732	0.2020
13 clean	39.18241	107.80258	2679	0.99944	1.098	0.0400
13	39.18241	107.80258	2679	0.99944	0.09601	0.0407
14	39.18073	107.80232	2679	0.99944	-0.2399	0.1870
20	39.22752	107.84286	2366	0.99967	0.09579	0.7530
22	39.22752	107.84286	2366	0.99967	0.3153	0.4940
36	39.18317	107.79922	2646	0.99888	0.5816	0.0297

The wide range of crushed ^{3}He/^{4}He is plotted in Figure 3.12, which indicated variability in the contribution of magmatic ^{3}He upon solidification of the basalt. For lobe P1, the average magmatic contribution for samples 13d, 14, and 36 was used in cosmogenic age determinations. For lobe P2, sample 7 was used because of its high fraction crush value when compared to sample 5. With more ^{3}He released upon crushing, the magmatic ^{3}He/^{4}He ratio was better estimated for samples with a higher fraction crush value. For lobe LV, an average of the values from the other two lobes (P1 and P2) was used for magmatic contribution, as the fraction crush values are too small to be reliably used in this way (Table 3.4). For lobe LV, the uncertainties for P1 and P2 were added.

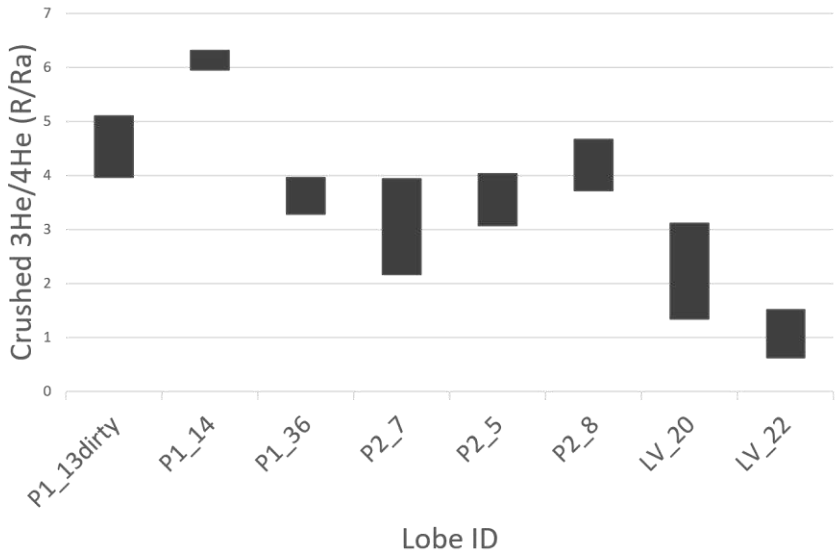

Figure 3.12 Crushed ^{3}He/^{4}He measurements.

The outputs from the Cronus calculator are shown in Table 3.6 and Figure 3.13. Sample 14 was not included in Table 3.6, because its crush $^3He/^4He$ ratio is larger than its melt $^3He/^4He$ ratio, resulting in a negative age estimation.

Table 3.6 Age dating results for ^3He cosmogenic nuclide samples, with the magmatic contribution to ^3He abundances is already subtracted.

Lobe ID	Sample ID	Age (kyr)	Analytical Uncertainty (kyr)	Total Uncertainty (kyr)
P1	13 clean	13.5	0.50135	1.9
P1	13	12.5	0.50599	1.8
P1	36	9.2	0.54871	1.5
P2	5	12.1	0.73595	1.8
P2	7	13.8	2.27190	2.8
P2	8	30.0	1.42910	4.0
LV	20	17.0	6.66430	7.0
LV	22	20.4	2.04910	3.2

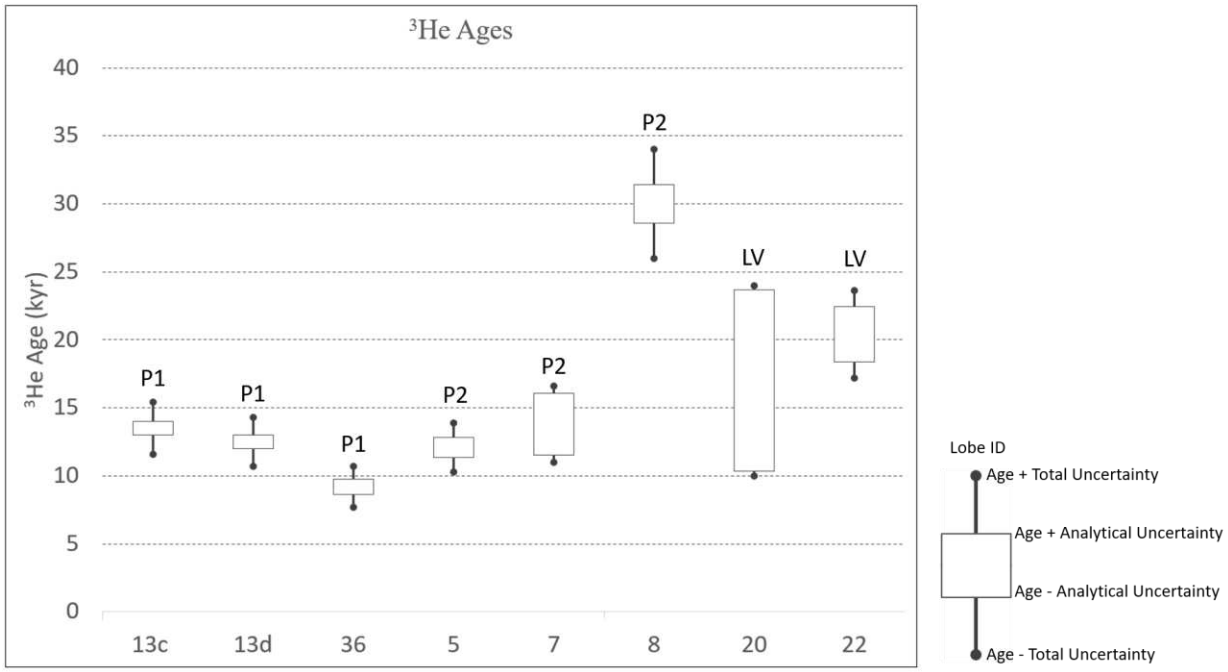

Figure 3.13 A graphical representation of the data in Table 3.6. Cosmogenic ages with the analytical and total uncertainties plotted. 13d refers to the sample in which the abrasion technique was applied to test for radiogenic contamination.

The results suggested that lobes P1 and P2 deposited within a short enough time period to be detectable by cosmogenic nuclide dating. The dates for 13d, and 36, on lobe P1, did not overlap using the analytical uncertainty. They did overlap when using the total uncertainty.

Since these samples were taken in very close proximity and on the same lobe, this was suggestive that the analytical uncertainty was too small to estimate the true age of a single lobe. Sample 13c, which was abraded in order to remove radiogenic contamination, should not be compared to the other sample dates since it was the only sample to undergo this methodology. An outlier did exist, sample 8, for lobe P2. This sample was much older than the other samples for P1 and P2. Therefore, inheritance was expected in this sample and it was not used in evaluating the relative ages of lobes P1 and P2. Ages for samples 5 and 7, on lobe P2, do overlapped even when using the analytical uncertainty. Additionally, the ages for samples 5 and 7 both overlapped with the age of 13d using the analytical uncertainty. Therefore, lobes P1 and P2 were likely deposited at the same time according to cosmogenic dates because most of the sampled ages overlapped using analytical uncertainty, and all of the sampled ages overlapped using total uncertainty.

Lobe LV was estimated to be older than the Park Deposit lobes using cosmogenic ages. Although the age of sample 20 overlaps with the Park Deposit samples (except sample 8 with its inherited signal), the analytical uncertainty of sample 20 was very large (6.7 kyr) because of the very small fraction crush value (Table 3.4). Sample 22 was a better estimate of the age of lobe LV because of its higher fraction crush value. Using either the analytical or total uncertainty, sample 22 had an age estimation that did not overlap any of the Park Deposit age estimations.

3.3 Relative Dating

The results for the relative dating techniques are reported in the following sections.

3.3.1 Schmidt Hammer Rebound Values

Schmidt hammer rebound value distributions, quantiles, and summary statistics are shown graphically on a lobe by lobe basis (Figure 3.14). The median and average rebound values are tabulated in Table 3.7.

Table 3.7 Basic Schmidt Hammer rebound value statistics.

Lobe ID	Median Rebound Value	Average Rebound Value
P1	49	48
P2	50	50
P3	53	51
P4	51	52
L1	44	44
L2	48	48
L3	51	49
L4	X	X
LV	45	44

The distributions of the Schmidt Hammer readings are roughly bell curves (Figure 3.14). The p-value results from the t-test using these distributions are reported in Table 3.8, and the means, standard deviations, standard errors, and sample counts reported in Figure 3.14 under summary statistics. Using a p-value threshold of <0.0500 to indicate populations of differing ages, in conjunction with average and median values from Table 3.7, suggested that the Park lobes should all be considered the same age. Even though lobes P1 and P4 had a p-value of 0.0285, Schmidt Hammer data from the other lobes were used. For example, lobes P1 and P2 had a p-value of 0.1963, suggestive that these populations should be considered from the same set of data. Lobes P4 and P2 had a p-value of 0.3832 and should also be considered from the same set of data. Therefore, if P1 was equal to P2, and P2 was equal to P4, then P1 was likely equal to P4.

For the Leon Deposit, the Schmidt Hammer data suggested two distinct populations of data which suggested two depositional events within the Leon Deposit. Lobe pairs L1 and L2, and L1 and L3, had p-values that are below the threshold of 0.0500, suggestive that L1 was from a different population than L2 and L3. Lobe pair L1 and LV, and L2 and L3, in contrast, had a p-value well above 0.0500. Therefore, Lobe pairs L1 and LV were the same age, and lobes L2 and L3 were the same age. The median and average values for these lobes showed that L2 and L3 have higher Schmidt Hammer rebound values than lobes L1 and LV, and therefore, L1 and LV were older than lobes L2 and L3.

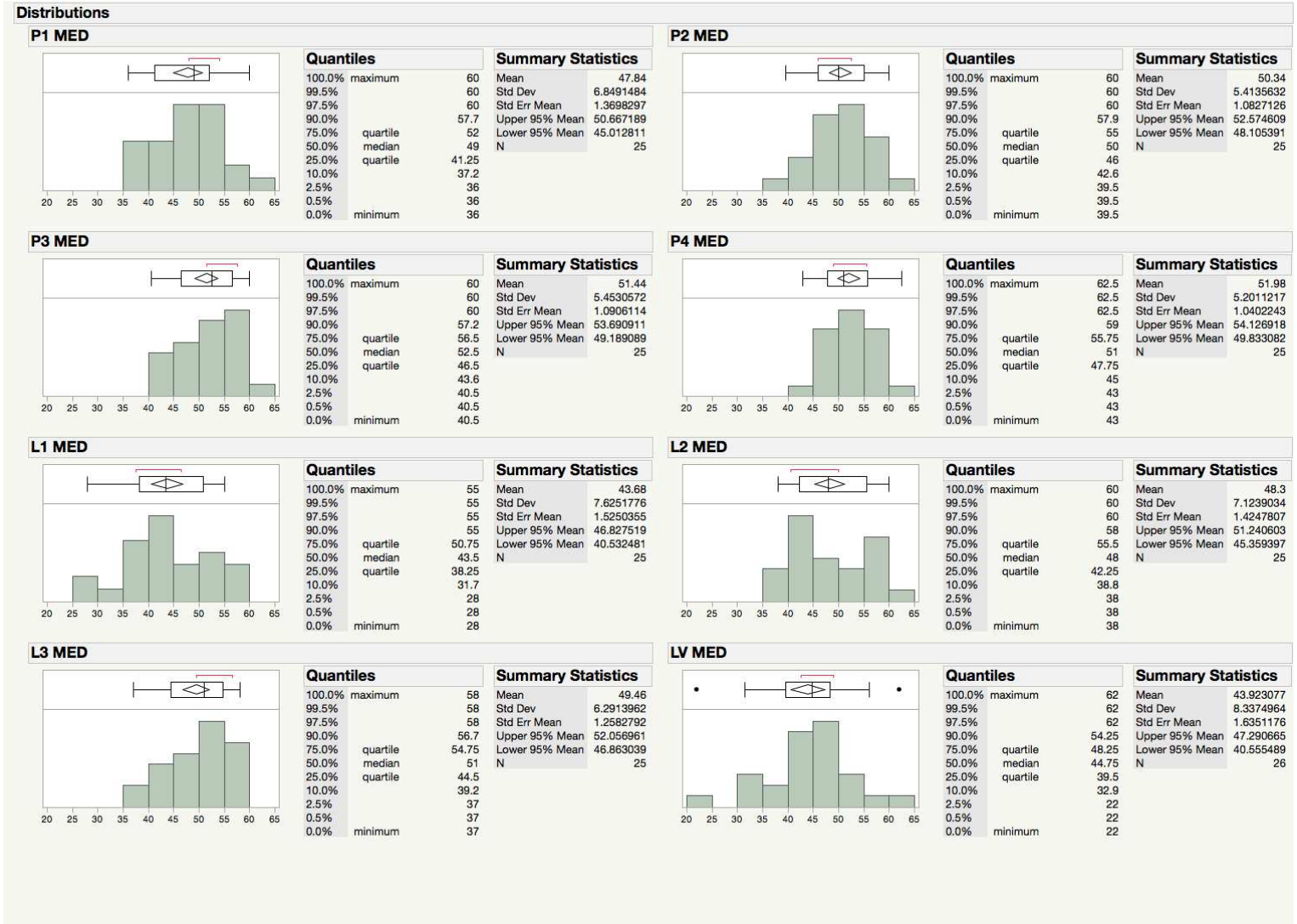

Figure 3.14 Schmidt Hammer rebound distributions.

Taken together, the Schmidt Hammer populations suggests that lobes L1 and LV first deposited, followed the rest of the lobes (on both the Park and Leon Deposit) in a short time period. Hence, lobes L2 and L3 have Schmidt Hammer populations that cannot be distinguished from the Park Deposit lobes.

Table 3.8 p-values from the results of the t-tests. Values less than 0.0500 are in red. Values between 0.0500 and <0.1000 are in orange to indicate lobe pairs that almost met the criteria necessary to be considered lobes of differing ages. All over values are in black.

	P1	P2	P3	P4	L1	L2	L3	LV
P1	X	0.1963	0.0635	0.0285	0.0323	0.8116	0.4017	0.8988
P2	0.1963	X	0.5689	0.3832	0.0007	0.2913	0.6485	0.0010
P3	0.0635	0.5689	X	0.7738	<0.0001	0.1051	0.3056	0.0001
P4	0.0285	0.3832	0.7738	X	<0.0001	0.0513	0.1808	<0.0001
L1	0.0323	0.0007	<0.0001	<0.0001	X	0.0176	0.0031	0.8988
L2	0.8116	0.2913	0.1051	0.0513	0.0176	X	0.5480	0.0230
L3	0.4017	0.6485	0.3056	0.1808	0.0031	0.5480	X	0.0042
LV	0.8988	0.0010	0.0001	<0.0001	0.8988	0.0230	0.0042	X

3.3.2 Rind-thickness Development, Pit Depths, and Lichenometry

We found that rinds did not form uniformly, whether on the surface or buried rocks. Development of rinds was very localized to discontinuities or convergent areas. On some samples a surface rind was suspected because of surface discoloration, however upon splitting or drilling of the rock, the rind would have no visible thickness. A varnish was found on some rocks that was uniform (Figure 3.15). However, the varnish was very light yellow in color, and not suspected to be have formed due to oxidation of iron bearing minerals. Therefore, measurements of rinds were not undertaken for the purposes of a relative age indicator.

Figure 3.15 Example of desert varnish.

Pit depths were analyzed on lobes P1, P2, L1, and L3 to test the potential applicability of the method. The count for the percentage of non-pitted rocks, and the average and median depth of the largest 6 pits are shown in Table 3.9. The results suggested that P1 was older than P2, which did not agree with the absolute dating method results (Figures 3.7, 3.8, and 3.13). The magnitude of the differences in the sizes of the pits was on the order of several mm. With the very little variability seen in the pit sizes, this method was not valid to distinguish relative ages for the Park and Leon Deposit lobes. Additionally, since the ratio of pitted versus nonpitted rocks did not correlate to the absolute dating methods, it was concluded that a variable other than ones related to age, such as initial vesicularity, governed this ratio.

Table 3.9 Pit-depth data.

	P1	P2	L1	L3
% not pitted	76	44	58	64
Average depth of top 6 (mm)	25.8	22.6	22.6	17.6
Median depth of top 6 (mm)	23.6	21.5	19.7	17.6

Figure 3.16 Example of desert varnish.

The lichen species present were not suitable for the age of the deposits in question. Radiocarbon ages, which were much younger than the cosmogenic ages, were between 500 and 4500 years old. The species present, such as xanthoparmelia, xanthoria, and lecanora novomexicana, only last less than 1000 years. Therefore, these species did not reach the necessary age to be useful in relative age estimations for these deposits. Ideal species such as rhizocarpon geographicum were not spotted on any of the deposits. Therefore, lichenometry was not completed.

CHAPTER 4

DISCUSSION

Each relative and absolute dating method implemented into this study came with its own set of assumptions and uncertainties. In order to interpret the data, all the results were evaluated together to provide for the best judgement of the true deposit ages and depositional origin. Results from each method are evaluated and discussed in the following sections.

4.1 Field and Desktop Mapping

Geometric analysis of the lobes shows that they have mobility indices that are much smaller than WSCL if the lobes are considered to have deposited contemporaneously (Table 3.1). WSCL has a mobility index of 0.14, whereas the Park and Leon Deposits both have a mobility index of 0.055. This indicates that the Park and Leon Deposits were much more mobile than the WSCL. The Oso Washington failure, with its mobility index of 0.10, is considered a much more frictional flow than the Park and Leon Deposits using this metric. Therefore, it is likely that the rheology of the Park and Leon Deposits differed greatly from that of WSCL and the Oso failure (Question #1 and Hypothesis #1).

It was also expected that field mapping could provide indications of whether the Park or Leon Deposits were of debris flow origin, as suspected by some previous researchers, or of glacial origin, as suspected by others. Geomorphic features suggestive of debris flow deposition, such as levees or a coarse snout, were not found in the Park and Leon Deposits. The lobes are not suspected to be levees because they have a variety of widths and lengths. It is suspected that if the lobes are actually levees, there would be more symmetry to their form. For example, if lobe P1 is a lateral levee, it is suspected by the author that there would be a lobe that matches P1 in its width and length in the same valley. Since this lobe is much larger than the other lobes within the Park Deposit, it does not appear that lateral levees are present.

Geomorphic features suggestive of glacial deposition, in contrast, were present but not common. The features interpreted as kettles were found frequently on the Park Deposit lobes.

Although no glacial striations were found on the boulder-rich deposits, they would not be common on boulders carried within the ice mass. Striations were present on the toreva blocks atop the Mesa, but not present over much of the glacial sediment in the region because of the unique setting that the Grand Mesa offers. The large flat area at high elevations allowed for the formation of the ice cap on the mesa that was not carving cirques or striations in the rocks like a glacier would in a mountainous region (Yeend, 1969). The Park Deposit ranges from 9300 - 7800 ft (2835 - 2377 m) asl, and the Leon Deposit ranges from 8600 – 7400 ft (2621 – 2256 m) asl, so both are located well above the conservative estimate of 6561 ft asl for the minimum ice tongue elevations (Cole and Sexton, 1981).

Terminal moraines were not found on either the Park or the Leon Deposits, which would not be expected if these were ground moraine and recessional deposits higher than the glacier terminus. Yeend (1969) describes the ice tongues as having extended much past the Park Deposit and into Plateau Creek to the north. Additionally, the head of the Park Deposit looks much the same as the rest of the deposit, with a boulder rich and lobate morphology. The lobes are continuous, with no obvious breaks in morphology from head to toe, so it is possible that the same depositing agent for the sediment at the head applies to the toe for this deposit. Lobe P1 extends to the Grand Mesa surface, where it is suspected to be in the area of the most ice accumulation for the region because of the relatively higher elevation and convergent topography (Yeend, 1969). Therefore, since the lobes are a continuous landform from head to toe, it is likely that the toe was also under ice.

The Leon Deposit lobes are very similar in form to the Park Deposit lobes. The lobes on both deposits are linear and rich in basalt boulders. Even in the non-lobate regions of Leon, where the land is very flat, shallow digging revealed basalt cobbles. There is no in-place basalt bedrock this far from the Grand Mesa surface, so the Leon Deposit is likely not bedrock as some authors have suggested. Field mapping suggests that Leon and Park have the same driving force because of the geometric and grain size similarity of the two deposits. Both the Leon and Park Deposit consist of lobate landforms of a variety of widths and lengths that each covered much of the valley. These lobes are adjacent to one another, with most of the boulders located on the convex portion of the lobes, and lack a coarse snout. The lobes do not appear to be altered since deposition, with little or no soil development or erosion. The matrix of the deposits are all very

similar, consisting of mostly fine grains smaller than sand and cobbles to boulder sized basalts. These similarities are suggestive of the same driving force.

4.2 Absolute Dating

4.2.1 Radiocarbon Dating

The analysis of the range of ages of organic compounds in the samples suggests that there was not a wide range of ages in the bulk organic content of the sediment. This conclusion is supported by comparison of humin and bulk organic dates. Sample P22H, which was dated using humin and not bulk organics, is 113 years older than the bulk organic date. In contrast, sample P23H, which was also dated using humin and not bulk organics, is 146 years younger than the bulk organic date for that sample (Figure 3.7). Since one humin date is older (P22H) and one is younger (P23H) than the corresponding bulk organic date, it is thought that most of the organic matter present fall into the narrow age range between the range of humin dates.

Although it is more common for the humin dates to reflect the age of the oldest organic compounds present, sometimes the opposite may occur. One possibility for humin dates to be younger than bulk organic dates is when organisms older than the feature itself produced significant humic and fulvic acids. These are removed for humin dating, so the sample appears younger than if they were left in the sample as is the case for bulk organic dating. Additionally, humin dates can yield problematic results depending on localized soil geochemistry. Many times, depending on the clay concentration, and if the younger or older humic/fulvic acids are bound to clay particles, the alkali extractions may preferentially remove the original or older labile carbon and leave behind the younger clay-bound humic and fulvic acids, or vice versa.

Radiocarbon dates suggested two depositional events for the Leon Deposit (Question #3 and Hypothesis #3). Lobes L1 and L4 first deposited around 3973 BP, which is the average of all L1 and L4 samples. In contrast, radiocarbon dating suggested lobes L2 and L3 were deposited much later, around 2415 BP. On the other hand, radiocarbon dates suggested the Park Lobes were deposited in one depositional event around 1638 BP (Question #3 and Hypothesis #3). These dates also suggest that the Leon Deposit was in place before the Park Deposit.

Uncertainties that are difficult to quantify were present on all the radiocarbon samples. Therefore, although not all the time intervals overlapped for all Park samples using 95%

confidence intervals even within a single lobe (Figure 3.8 and Table 3.2), only quantifiable uncertainties were incorporated in the Oxcal software results. Furthermore, since bulk sediment was dated and not a macroparticle, with a range of organic matter of varying ages, there are additional uncertainties that should be considered.

Some of these uncertainties, such as the ones due to incorporation of present-day organic matter, are suspected to have occurred at comparable rates for all samples on each lobe. This is because of the proximity of the samples to each other, the similarity of vegetation/animal activity, and the lack of soil development on each lobe. Therefore, the ages of the lobes presented here are expected to accurately reflect the depositional sequence, but not necessarily the true age of the deposit since some of the uncertainties are not quantified.

4.2.2 Cosmogenic Nuclide Dating

Cosmogenic dates yield the same overall conclusions as the radiocarbon dates showing similar ages of lobes P1 and P2 (samples 13c, 13d, 36, 5, and 7 in Figure 3.13 and Table 3.6) (Question #3 and Hypothesis #3). The dates for lobe LV (samples 20 and 22 in Figure 3.13 and Table 3.6) are older than those for P1 and P2, which is also indicated by the radiocarbon dates (Figure 3.7 and Table 3.3). In order to have a robust cosmogenic nuclide dating program, samples were submitted for analysis in small sets to investigate if inheritance would be detrimental to the technique. Unfortunately, the stepwise approach resulted in the first set taking in excess of two years to receive results. Therefore, this step-wise approach fell outside of the time frame allotted to this project, so only three samples were analyzed.

Several criteria were used to judge the validity of the cosmogenic nuclide dating results and remove some samples from further consideration. First, radiogenic contamination should be suspected under the following conditions: if the melt $^{3}He/^{4}He$ ratio was lower than the crush ratio, if the $^{3}He/^{4}He$ crush ratio was lower than 1 (Cerling 1999), and/or if the abraded sample returned an older age than the unabraded sample. Since the melt $^{3}He/^{4}He$ ratio was lower than crush ratio for sample 14, this sample was not able to be dated. Additionally, the abraded sample 13 returned a younger age (13.5 kyr) than the unabraded sample (12.5 kyr), and therefore it was suspected that radiogenic contamination was present, which could make the samples appear

approximately 8% older than the true boulder age for the basalts in this region. Therefore, the value for sample 13 was used with caution.

Additionally, it is necessary to have a relatively high "fraction crush" value, indicating enough ^{3}He was released upon melting to provide a valid measurement (Table 3.4). A low fraction crush value indicates that upon melting, a very little amount of helium was released compared to the total helium in the sample. No magnitude could be found in the literature as to what constitutes a high enough fraction crush value, however, samples 5, 20, and 22 all have fraction crush values below 1%. Therefore, caution should be used when evaluating the results from those samples.

Sample 5, on lobe P2, has an age determination that matches well with the other Park Deposit samples, and is therefore probably valid. Samples 20 and 22 on lobe LV compare well with each other and also match radiocarbon and Schmidt Hammer conclusions that lobe LV is much older than the other lobes.

Lastly, it is desirable to have a $^{3}He/^{4}He$ melt ratio above 6-8 Ra because at ratio below that would match mantle values too closely. This is common in rocks where the formation age is much greater than the exposure age, which is the case here (Marrero et al., 2015). Samples 14, 20, and 22 has melt $^{3}He/^{4}He$ ratios under this threshold. While sample 14 was already eliminated from consideration for other reasons noted above, and samples 20 and 22 should only be used with caution.

The cosmogenic nuclide ages presented in Table 3.6 are likely an overestimate of the true deposit age. This is due to radiogenic contamination and snow shielding. New cosmogenic nuclide ages for the deposits are estimated in Table 4.1 incorporating the 8% underestimation of the true age due to radiogenic contamination and 12% underestimation of the age from snow shielding (Benson, 2004). The incorporation of the radiogenic contamination and snow shielding does not change the relative ages of the deposits, and only changes the absolute ages by a small amount.

Using Table 4.1, the best estimate for the Park Deposit is an average of all P1 and P2 samples excluding sample 8, which has inheritance issues. This results in an age of approximately 14.3 kyr for the Park lobes. The best estimation for the age of LV is from sample

22, since sample 20 has such a large uncertainty (Figure 3.13). This results in an age of 24.4 kyr for LV. These estimates incorporate the radiogenic contamination and snow shielding effects.

Table 4.1 New estimation of cosmogenic nuclide sample ages with the incorporation of a 8% underestimation of the Cronus age from radiogenic contamination and a 12% (Benson, 2004) underestimation of the Cronus age from snow shielding.

Lobe ID	Sample ID	Cronus Age (kyr)	Radiogenic Contamination estimate of 8% of the Cronus age (kyr)	Snow shielding estimate from Benson (2004) of 12% of the Cronus age (kyr)	New age determination incorporating radiogenic contamination and snow shielding (kyr)
P1	13 dirty	12.5	+1.0	+1.5	15.0
P1	36	9.2	+0.7	+1.1	11.0
P2	5	12.1	+1.0	+1.5	14.6
P2	7	13.8	+1.1	+1.7	16.6
P2	8	30.0	+2.4	+3.6	36.0
LV	20	17.0	+1.4	+2.0	20.4
LV	22	20.4	+1.6	+2.4	24.4

4.3 Relative Dating

Schmidt Hammer rebound values are the most reliable relative dating metric used in this study for the region. The conclusion for relative ages of the deposits for the Schmidt Hammer data is in agreement with the radiocarbon and cosmogenic nuclide dating results. Schmidt Hammer data leads to the estimation that lobes L2 and L3 are the same age, which agrees with radiocarbon dating results. Additionally, Schmidt Hammer data leads to the estimation that all Park Lobes were deposited at the same time, which agrees with radiocarbon dating conclusions (Question #3 and Hypothesis #3) and cosmogenic nuclide dating results. Lastly, Schmidt Hammer data suggests that lobe L1 is older than lobes L2, L3, and all Park Lobes, which agrees with relative age estimations using radiocarbon dating.

No weathering rind was observed for most of the measured rocks. Since erosion of the outer layer of the basalts is not suspected to have removed any rinds, we conclude that the deposits are too young to have developed rinds in the first place. Yoshida et al. (2011) calculated an average rind formation rate of 5 mm/100 ka for basalts. However, the youngest deposits analyzed by that study were 50 ka. Colman (1981) created rind development curves for basalt and andesite (Figure 4.1). This figure suggests a lag time between deposition and the start of rind formation on the order of 10,000 years. Therefore, it is suspected that the deposits on Park and Leon, lacking weathering rinds, are not significantly older than 10,000 years (also confirmed by cosmogenic and radiocarbon dates).

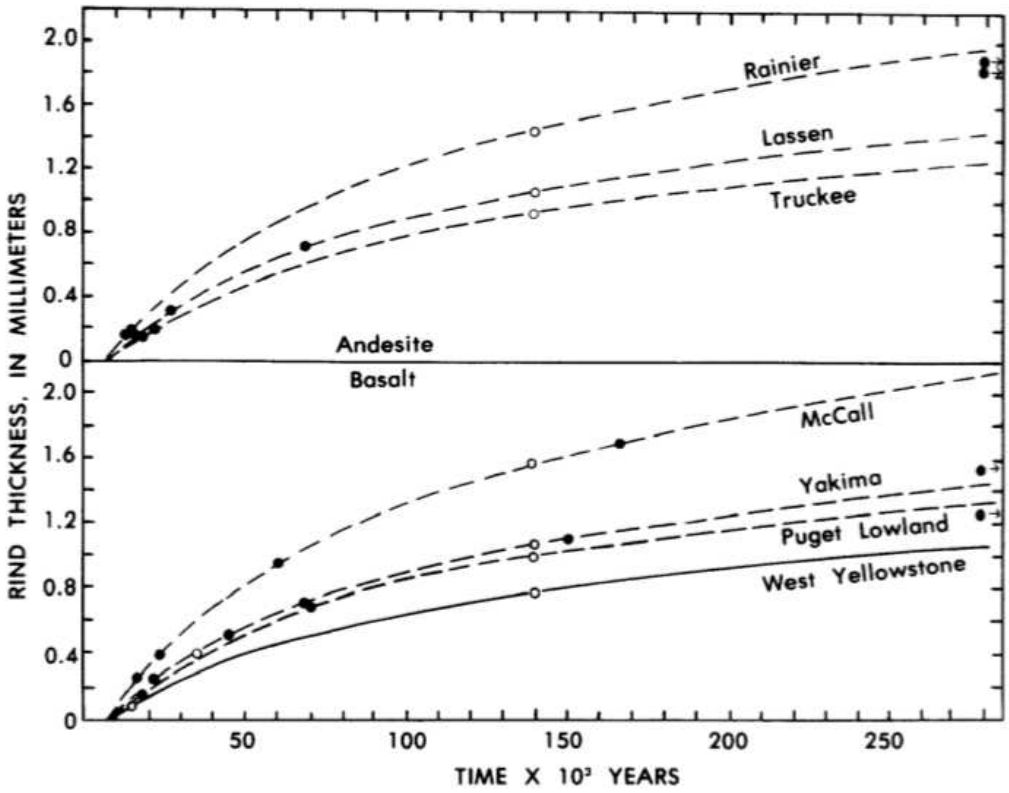

Figure 4.1 Weathering rind thicknesses of basalts in western United States (Colman, 1981).

Likewise, lichenometry and pit depth measurements did not work in this area. The species of lichen that are present are only good for deposits of much younger age than the estimated ages for the Park and Leon deposits. Pit depths and pitted to nonpitted ratios are too variable and also do not reflect relative ages of the deposits.

4.4 Origin of Deposits and Their Usefulness in WSCL-like Hazard Assessments

Several lines of evidence point towards the Park and Leon Deposits being of glacial origin, not a gravitational mass failure origin, creating enough uncertainty in their origin that they should not be used in hazard assessments of mass failure for this region (Question #1 and #2; Hypotheses #1 and #2). Although mapped previously by Soule (1988) as debris flows, our detailed field mapping failed to locate diagnostic debris flow landforms, such as levees or a bouldery snout.

On the other hand, there are lines of evidence supporting glacial origin for these two deposits (Hypothesis #4). First, our field mapping identified kettles on the Park Deposit at low elevations, which are common in glacial terrain but not on debris flow deposits. Glacial origin is also indicated by the continuity of the Park deposit to higher elevations on top of the mesa, where glacial striations are present. Although kettles and striations were not found on the Leon Deposit, the lobes have the same form as the Park Deposits and are presumably deposited by the same mechanism. All the Park and Leon Deposit lobes are linear in shape, and their crests and troughs have about the same elevation differences for each lobe. The lobes are mainly adjacent to other lobes with little flat land between them. Lastly, the combination of radiocarbon and cosmogenic nuclide dates reveals a lag time present between deposition and the accumulation of datable organic matter, suggestive of a glacial origin. This lag time will be discussed below.

With the large magnitude of these deposits, it is reasonable to suspect the radiocarbon age provides a maximum age of the deposits if they are of debris flow origin because a lag time would not dominate the age of organics in the deposits. This is especially true for a large debris flow deposit that has not been altered by soil formation after deposition. A large debris flow would incorporate carbon from its path into the deposit in a short amount of time, such as at the WSCL. These organics would either be the age of the flow (vegetation killed by the flow) or older than the flow (organics entrained that had already died). Since there is little evidence of alteration of the deposit since its deposition, the accumulation of recent organics that would drastically change the radiocarbon age of the sediment in the deposit seems unlikely. Cosmogenic ^{3}He begins accumulating immediately after debris flow deposition, so radiocarbon dates would likely reflect the same age or an older age than cosmogenic nuclide ages of the same debris flow deposit, if cosmogenic inheritance is not suspected.

In contrast, it is reasonable to suspect that radiocarbon dating provides a minimum possible age for a glacial deposit due to a lag time that is present between deposition and accumulation of datable organic matter. For Pinedale glaciation, which is suspected in our area, the lag time between the retreat of the glacier and the accumulation of datable organic matter can be hundreds to thousands of years depending on location (Balco et al., 2011). Since cosmogenic ^{3}He would begin accumulating immediately after the ice melting, radiocarbon dates would likely reflect a younger age than the cosmogenic nuclide ages for the same glacial deposit due to this lag time.

Since the cosmogenic age calculations are much older than the radiocarbon dates for these deposits, it supports the interpretation that the Park and Leon deposits are of glacial origin (Hypothesis #4). For example, for lobes P1 and P2, which have both radiocarbon and cosmogenic nuclide data, the cosmogenic dates are on the order of thousands of years older. The lag time is considered accurate since the humin dates suggest a narrow range for the ages of the organic compounds present in these samples. Additionally, although no lobes on the Leon Deposit were dated for both cosmogenic nuclide and radiocarbon ages, the Schmidt Hammer rebound values suggest lobe LV, which was dated using cosmogenic nuclide dating, and lobe L1, which was dated using radiocarbon dating are the same age. Radiocarbon dates for lobe L1 had an average date of 3668 BP (Table 3.3). The best cosmogenic nuclide date for lobe LV is 24.4 kyr (Table 4.1). Therefore, a very large lag time exists in the lobe LV as well, suggestive of a glacial origin for this lobe.

Since lobes L1, L4, and LV are the same age, they are all possibly glacial deposits because of the lag time present in the radiocarbon dates. Lobes L2 and L3 appear younger than the lobes L1, L4, and LV, and therefore, the same lag time may not be present for these lobes. However, lobes L2 and L3 are the same age as the Park Lobes as concluded in section 5.3.1 with Schmidt Hammer data analysis. Additionally, Figure 3.7 shows that the range of radiocarbon dates seen on lobes L2 and L3 overlap with the Park Deposit age ranges. Since the Park Deposit is likely late Pinedale glaciation, it is also likely that lobes L2 and L3 are as well. Lobes L1, L4, and LV correspond in timing to around the maximum extent of Pinedale glaciation estimated to be 22.4 +/- 1.1 BP (Benson, 2004). Therefore, it is suspected that sometime around maximum

extent, there were two episodes of extreme melting in this region, one that deposited lobes L1, L4, and LV, and a later one that deposited lobes L2, L3, and the Park Lobes.

If debris flow in origin, the radiocarbon dates are likely the correct absolute ages for the deposits for the reasons stated earlier in this section, which does not change the relative ages of the deposits. If debris flow in origin, then the cosmogenic ages would be older than the radiocarbon ages because of an inherited cosmogenic signal. Since the cosmogenic dates reflect the end of Pinedale glaciation for the Park Deposits and 2 of the Leon Deposit lobes, this suggests that the debris flows were not erosive enough to remove this inherited cosmogenic signal. However, it seems unlikely that no boulders would be dated with ages younger than Pinedale glaciation if this were the case. Therefore, I maintain the hypothesis that these deposits are Pinedale glacial deposits.

Assuming these are glacial deposits, the next question to answer is whether they are glacial moraine or outwash. Stratification, which would indicate that they were outwash, was not found within the Park or Leon deposits. Additionally, the very linear form of the deposits was more indicative of a moraine than of outwash. Therefore, glacial moraine origin is suspected.

Since the origin of the Park and Leon Deposits is at best questionable, and more possibly a glacial moraine than a debris flow deposit, they should not be used in modern day hazard assessments for the region, such as in East Salt Creek (Question #1 and Hypothesis #1). They offer no insight into the magnitude/recurrence interval relationship of gravitational mass failures for this region. Although we agree with the boundaries drawn by Soule (1988) for these deposits, we disagree that their origin is “old debris flow” deposits. Therefore, it is recommended that this map be used with caution for predicting future hazards, and the units mapped as “old debris flow” should be reexamined to confirm their depositing mechanism.

CHAPTER 5

CONCLUSIONS

Mapping, absolute and relative dating methods suggests that the Leon and Park Deposits are of glacial origin and not of debris flow origin as Soule (1988) mapped. Therefore, these deposits should not be used in hazard assessments of future gravitational mass failures (Hypothesis #1), and gravitational mass failures are not as prominent as the Soule (1988) map suggests (Question #4 and Hypothesis #4). Even if debris flow in origin, these deposits occurred either shortly after the maximum Pinedale ice extent or after ice melting, and therefore, the climate has changed significantly since deposition (Hypothesis #2). The Leon Lobes were deposited first, followed by the Park Lobes. The Leon lobes were deposited in two events as suggested by radiocarbon data, with lobes L1, L4, and LV first depositing, and then lobes L2 and L3 (Question #3 and Hypothesis #3). The Park Lobes were deposited within a very short time period by melting ice, and we cannot statistically say that the lobes are of different ages using either radiocarbon ages, cosmogenic nuclide ages, or Schmidt Hammer data (Question #3 and Hypothesis #3). Using both cosmogenic nuclide and radiocarbon dates shows that radiocarbon dates should be considered a relative dating method for this region, since there is a lag time between ice melting and carbon accumulation in the deposit. Schmidt Hammer rebound values agree with the relative ages in radiocarbon and cosmogenic nuclide dating and offer a low cost and quick method for estimating relative ages of glacial deposits in the Grand Mesa region. Alternatively, with more cosmogenic and radiocarbon dates from the same deposits in this region, the lag time could be more narrowly defined, which would allow radiocarbon dating of bulk sediment to be used as a quick and cost-effective absolute dating technique compared to cosmogenic nuclide dating.

REFERENCES

Balesdent, J. (1987). The turnover of soil organic fractions estimated by radiocarbon dating. *Science of the Total Environment*, *62*, 405-408.

Baum, R. L., & Odum, J. K. (1996). Geologic map of slump-block deposits in part of the Grand Mesa area, Delta and Mesa Counties, Colorado. *US Geological Survey Open-File Report*, *96*(017), 12.

Becker-Heidmann, P., Liang-wu, L., & Scharpenseel, H. W. (1988). Radiocarbon dating of organic matter fractions of a Chinese mollisol. *Zeitschrift für Pflanzenernährung und Bodenkunde*, *151*(1), 37-39.

Benedict, J. B. (1968). Recent glacial history of an alpine area in the Colorado Front Range, USA: II. Dating the glacial deposits. *Journal of Glaciology*, *7*(49), 77-87.

Benson, L., Madole, R., Phillips, W., Landis, G., Thomas, T., & Kubik, P. (2004). The probable importance of snow and sediment shielding on cosmogenic ages of north-central Colorado Pinedale and pre-Pinedale moraines. Quaternary Science Reviews, 23(1-2), 193-206.

Blard, P. H., Lavé, J., Sylvestre, F., Placzek, C. J., Claude, C., Galy, V., ... & Tibari, B. (2013). Cosmogenic ^{3}He production rate in the high tropical Andes (3800 m, 20 S): Implications for the local last glacial maximum. *Earth and Planetary Science Letters*, *377*, 260-275.

Burbank, D. W., & Cheng, K. J. (1991). Relative dating of Quaternary moraines, Rongbuk Valley, Mount Everest, Tibet: implications for an ice sheet on the Tibetan Plateau. Quaternary Research, 36(1), 1-18.

Carrara, P. E., & Andrews, J. T. (1973). Problems and application of lichenometry to geomorphic studies, San Juan Mountains, Colorado. Arctic and Alpine Research, 5(4), 373-384.

Carroll, T. (1974). Relative age dating techniques and a late Quaternary chronology, Arikaree Cirque, Colorado. *Geology*, *2*(7), 321-325.

Cerling, T. E. (1990). Dating geomorphologic surfaces using cosmogenic 3 He. *Quaternary Research*, *33*(2), 148-156.

Cerling, T. E., & Craig, H. (1994). Geomorphology and in-situ cosmogenic isotopes. *Annual Review of Earth and Planetary Sciences*, *22*(1), 273-317.

Cerling, T. E., Webb, R. H., Poreda, R. J., Rigby, A. D., & Melis, T. S. (1999). Cosmogenic ^{3}He ages and frequency of late Holocene debris flows from Prospect Canyon, Grand Canyon, USA. *Geomorphology*, *27*(1-2), 93-111.

Coe, J. A., Baum, R. L., Allstadt, K. E., Kochevar Jr, B. F., Schmitt, R. G., Morgan, M. L., ... & Kean, J. W. (2016). Rock-dynamics revealed by large-scale field mapping and seismic

signals at a highly mobile avalanche in the West Salt Creek valley, western Colorado. Geosphere, 12(2), 607-631.

Cole, R.D., Sexton, J.L. (1981). Pleistocene surficial deposits of the Grand Mesa area,Colorado, in Epis, R.C., Callender, J.F., eds., Western Slope Colorado: New Mexico Geological Society 32nd Field Conference Guidebook , p. 121–126.

Cole, R.D., Heizler, M., Karlstrom, K.E., and Stork, A. (2010). Eruptive history of the Grand Mesa basalt field, western Colorado (abs.): Geological Society of America Abstracts with Programs, v. 42, no. 5, p. 76.

Cole, R. D., Beard, L. S., Karlstrom, K. E., Young, R. E., & Billingsley, G. H. (2011). Significance of the Grand Mesa basalt field in western Colorado for defining the early history of the upper Colorado River. In CREvolution 2—Origin and evolution of the Colorado River system, workshop abstracts: US Geological Survey Open-File Report 2011–1210 (pp. 55-61).

Cole, R.D., Stork, A., and Hood, W.C. (2016). Geochemical variation of Grand Mesa Volcanic Field, western Colorado (abs): Geological Society of America Abstracts with Programs, v. 48, no. 7, Paper 315-5, doi: 10.1130/abs/2016AM-283767.

Cole, R.D., Stork, A., Hood, W.C., & Heizler, M. (2017). Geochemical and Geochronological Characterization of Grand Mesa Volcanic Field, western Colorado. Unpublished manuscript.

Colman, S. M. (1981). Rock-weathering rates as functions of time. *Quaternary Research*, *15*(3), 250-264.

Colman, S. M. & Pierce, K.L.(1981). Weathering rinds on andesitic and basaltic stones as a Quaternary age indicator, western United States. *US Geol. Surv. Prof. Paper*, *1210*, 56.

Craig, H., & Poreda, R. J. (1986). Cosmogenic ^{3}He in terrestrial rocks: The summit lavas of Maui. *Proceedings of the National Academy of Sciences*, *83*(7), 1970-1974.

Day, M. J., & Goudie, A. S. (1977). The Schmidt Hammer and field assessment of rock hardness. *Br. Geomorphol. Res. Group, Tech. Bull.*, *18*, 19-29.

Donnell, J. R., Yeend, W. E., & Smith, M. C. (1985). Preliminary geologic map of the Collbran Quadrangle, Mesa County, Colorado (No. 1825).

Evans, D. J. A., Archer, S., & Wilson, D. J. H. (1999). A comparison of the lichenometric and Schmidt hammer dating techniques based on data from the proglacial areas of some Icelandic glaciers. *Quaternary Science Reviews*, *18*(1), 13-41.

Ferguson, C. W. (1971, April). Tree-ring dating of Colorado River driftwood in the Grand Canyon. Arizona-Nevada Academy of Science.

Goehring, B. M., Kurz, M. D., Balco, G., Schaefer, J. M., Licciardi, J., & Lifton, N. (2010). A reevaluation of in situ cosmogenic ^{3}He production rates. *Quaternary Geochronology*, *5*(4), 410-418.

Hail, W.J, Jr.1(1972a). Reconnaissance geologic map of the Hotchkiss area, Delta and Montrose Counties, Colorado: U.S. Geological Survey Miscellaneous Geologic Investigations Map 1-698.

Hail, W.J., Jr. (1972b). Reconnaissance geologic map of the Cedaredge area, Delta County, Colorado: U.S. Geological Survey Miscellaneous Geologic Investigations Map 1-697.

Henderson, J. (1923). The Glacial Geology of Grand Mesa, Colorado. The Journal of Geology, 31(8), 676-678.

Hereford, R., Thompson, K. S., & Burke, K. J. (1998). Numerical ages of Holocene tributary debris fans inferred from dissolution pitting on carbonate boulders in the Grand Canyon of Arizona. Quaternary Research, 50(2), 139-147.

Iverson, R. M., George, D. L., Allstadt, K., Reid, M. E., Collins, B. D., Vallance, J. W., ... & Baum, R. L. (2015). Landslide mobility and hazards: implications of the 2014 Oso disaster. *Earth and Planetary Science Letters*, *412*, 197-208.

Kurz, M. D. (1986a). Cosmogenic helium in a terrestrial igneous rock. Nature, 320(6061), 435.

Kurz, M. D. (1986b). In situ production of terrestrial cosmogenic helium and some applications to geochronology. Geochimica et Cosmochimica Acta, 50(12), 2855-2862.

Laustela, M., Egli, M., Frauenfelder, R., Kääb, A., Maisch, M., & Haeberli, W. (2003). Weathering rind measurements and relative age dating of rockglacier surfaces in crystalline regions of the Eastern Swiss Alps. In *Permafrost: Proceedings of the Eighth International Conference on Permafrost* (pp. 627-632).

Lienkaemper, J. J., & Ramsey, C. B. (2009). OxCal: Versatile tool for developing paleoearthquake chronologies—A primer. *Seismological Research Letters*, *80*(3), 431-434.

Madole, R. F. (1986). Lake Devlin and Pinedale glacial history, front range, Colorado. *Quaternary Research*, *25*(1), 43-54.

Mahaney, W. C. (1973). Neoglacial chronology in the Fourth of July cirque, central Colorado Front Range. *Geological Society of America Bulletin*, *84*(1), 161-170.

Marrero, S. M., Phillips, F. M., Borchers, B., Lifton, N., Aumer, R., & Balco, G. (2016). Cosmogenic nuclide systematics and the CRONUScalc program. *Quaternary Geochronology*, *31*, 160-187.

Marvin, R. F., Mehnert, H. H., & Mountjoy, W. M. (1966). Age of basalt cap on Grand Mesa. *US Geological Survey Professional Paper*, *550*, 81.

Matthews, J.A., & Shakesby, R.A. (1984). The status of the 'Little Ice Age'in southern Norway: relative-age dating of Neoglacial moraines with Schmidt hammer and lichenometry. *Boreas*, *13*(3), 333-346.

McCarroll, D. (1987). The Schmidt hammer in geomorphology: five sources of instrument error. *British Geomorphological Research Group Technical Bulletin*, *36*, 16-27.

McCarthy, D. P., & Zaniewski, K. (2001). Digital Analysis of Lichen Cover: A Technique for Use in Lichenometry and Licnenology. *Arctic, Antarctic, and Alpine Research*, *33*(1), 107-113.

McSaveney, M. J. (1992). *A manual for weathering-rind dating of grey sandstones of the Torlesse Supergroup, New Zealand* (Vol. 92). Institute of Geological & Nuclear Sciences.

Nygren, W. E. (1935). An Outline of the General Geology and Physiography of the Grand Valley District (Doctoral dissertation, University of Colorado).

Pessenda, L. C. R., Gouveia, S. E. M., & Aravena, R. (2001). Radiocarbon dating of total soil organic matter and humin fraction and its comparison with 14 C ages of fossil charcoal. *Radiocarbon*, *43*(2B), 595-601.Sinnock, Scott, 1978, Geomorphology of the Uncompahgre Plateau and Grand Valley, western Colorado, U.S.A. (Ph.D dissertation): West Lafayette, Indiana, Purdue Universitym 196 p.

Retzer, J. L. (1954). Glacial advances and soil development, Grand Mesa, Colorado. American Journal of Science, 252(1), 26-37.

Shakesby, R. A., Matthews, J. A., & Owen, G. (2006). The Schmidt hammer as a relative-age dating tool and its potential for calibrated-age dating in Holocene glaciated environments. *Quaternary Science Reviews*, *25*(21-22), 2846-2867.

Soule, J. M. (1988). Surficial-geologic and landslide map of Vega Reservoir and vicinity, Mesa County, Colorado.

Sumner, P., & Nel, W. (2002). The effect of rock moisture on Schmidt hammer rebound: tests on rock samples from Marion Island and South Africa. *Earth Surface Processes and Landforms: The Journal of the British Geomorphological Research Group*, *27*(10), 1137-1142.

Wang, Z., Zhao, H., Dong, G., Zhou, A., Liu, J., & Zhang, D. (2014). Reliability of radiocarbon dating on various fractions of loess-soil sequence for Dadiwan section in the western Chinese Loess Plateau. *Frontiers of earth science*, *8*(4), 540-546.

White, J. L., Morgan, M. L., & Berry, K. A. (2015). The West Salt Creek landslide: a catastrophic rockslide and rock/debris avalanche in Mesa County, Colorado. Colorado Geological Survey Bulletin, 55, 45.

Williams, R. B. G., & Robinson, D. A. (1983). The effect of surface texture on the determination of the surface hardness of rock using the Schmidt hammer. *Earth Surface Processes and Landforms*, *8*(3), 289-292.

Winkler, S. (2005). The Schmidt hammer as a relative-age dating technique: potential and limitations of its application on Holocene moraines in Mt Cook National Park, Southern Alps, New Zealand. *New Zealand Journal of Geology and Geophysics*, *48*(1), 105-116.

Yeend, W. E. (1969). Quaternary geology of the Grand and Battlement. *Mesas area: US Geological Survey Professional Paper*, *617*, 49.

Yoshida, H., Metcalfe, R., Nishimoto, S., Yamamoto, H., & Katsuta, N. (2011). Weathering rind formation in buried terrace cobbles during periods of up to 300ka. *Applied geochemistry*, *26*(9-10), 1706-1721.